Early immunity to *Mycobacterium tuberculosis*: new insights into macrophage heterogeneity and vaccine-mediated responses

Jared L. Delahaye

A dissertation submitted in partial fulfillment of the requirements for the degree of
Doctor of Philosophy

University of Washington
2019

Reading Committee:
Kevin B. Urdahl, Chair
Jessica Hamerman
Martin Prlic

Program Authorized to Offer Degree:
Immunology

ABSTRACT

Early immunity to *Mycobacterium tuberculosis*: new insights into macrophage heterogeneity and vaccine-mediated responses

Jared L. Delahaye

Doctor of Philosophy in Immunology

University of Washington, 2019

Dr. Kevin B. Urdahl, Chair

Tuberculosis (TB), caused by the bacteria *Mycobacterium tuberculosis* (Mtb), kills more individuals than any other single infectious agent. The only approved vaccine, BCG, poorly prevents the spread of disease, highlighting the fact that new vaccines are needed to eradicate TB. These efforts would benefit from a mechanistic understanding of how immunity to TB can be achieved as well as insight into the barriers that restrict immunity. However, a number of gaps in our knowledge of TB immunity remain. In particular, the interaction between Mtb and its target cell, the macrophage, during the early stages of infection remains incompletely understood. Here, we characterized the distinct response programs which are initiated in lung-resident alveolar macrophages (AM) and lung-infiltrating monocyte-derived macrophages (MDM). We find that infected AM harbor many more Mtb bacilli than infected MDM during both the innate and adaptive phases of the immune response. Using RNA-seq, we identified multiple differentially expressed pathways between the two cell types. While infected MDM upregulate canonical proinflammatory signaling pathways associated with Mtb control, infected AM are enriched for pathways relating to proliferation and fatty acid metabolism. Additionally, a number of genes relating to phagosome maturation and nitric oxide production were also differentially expressed. However, validation studies using gene knockout animals did not

support a cell-intrinsic, protective role afforded by these genes. In addition to these host studies, we also investigated the transcriptional response of the Mtb itself. Here we found that Mtb in MDM have a transcriptional signature associated with late hypoxia, a known Mtb stress condition.

We next used a mouse model of prior BCG immunization in order to understand how this vaccine alters early Mtb immunity. Here we found that BCG promotes a dramatic shift in the cell types targeted for Mtb infection. While AM are the major infected cell for the first two weeks of Mtb infection in unimmunized animals, BCG promotes the accelerated transfer of bacteria into neutrophils and MDM. To determine the requirements for this transfer, we characterized the dynamics of the T cell response using tetramers. BCG-specific CD4 and CD8 T cells were present in the lungs of immunized animals prior to infection, and as early as D10 post-infection, there were 5-fold more of these cells compared to controls. Using T cell-depleting antibodies, we found that the transfer of infection out of AM was dependent on CD4, but not CD8, T cells yet did not require infected AM-intrinsic antigen recognition. Finally, using confocal microscopy, we saw that Mtb-specific T cells were first activated in lung regions devoid of infected cells. Importantly, these events preceded BCG-induced control of the bacterial burden, which occurred only after the co-localization of T cells and infected cells.

Together, these studies further our understanding of the early immune response to Mtb. Specifically, they show that the cell types targeted for infection differ profoundly in their ability to control Mtb. In addition, vaccination begins to shape immunity much earlier than previously appreciated by accelerating the infection of recruited macrophages, however, the delayed colocalization of T cells with infected cells in the lung represents a barrier to vaccine-induced immunity. These results could help to inform more rationale vaccine design for TB.

TABLE OF CONTENTS

LIST OF FIGURES

Chapter 3:

Chapter 4:

LIST OF TABLES

Chapter 3:

ACKNOWLEDGEMENTS

I thank Kevin for being an endlessly supportive mentor. I couldn't have imagined a better lab environment to call home these past years and I believe he deserves much of the credit for establishing that through his creativity and positivity. I started grad school with significant doubts about my scientific abilities. Kevin has always been available to discuss experimental details both big and small, and has helped me grow into a more confident researcher. I will forever be grateful for the opportunities he has given me to do exciting, meaningful science.

I thank Urdahl Lab members past and present for critical and experimental support. I thank Courtney for welcoming me into the lab and treating me with respect from day one. Whenever I've been concerned about an experiment or analysis going poorly, Courtney has always kept me calm and helped decide on the best steps to take. I thank Sara for spending more hours in the BSL3 with me than anyone else. Perhaps no one else was up to the task of putting up with me for that long. Thank you Sara for laughing maniacally with me when mice would escape from the bell jar, understanding all of my Lord of the Rings references, most of my Star Wars references, and tolerating the endless string of Seinfeld references. I thank Shahin for helping me to initiate multiple projects and immunize hundreds of mice. I thank Ben for working with me to generate absolutely gorgeous imaging data as well as answer all my weird medical questions. I thank Kristin for her bacterial expertise and help with many TB-BSL3 experiments. I thank our fantastic technician, Bridget, who keeps the lab running and has infected hundreds of mice for me in the past few months to help me get through revision experiments.

I thank our collaborators in the Gerner Lab and Baliga Lab (particularly Eliza and Chris). I thank members of the other TB research labs at CGIDR: the Sherman Lab, Grundner Lab, and Aderem Lab (particularly Alissa and Greg). I thank the members of my committee: Jess, Dan,

Martin, and Savan for keeping me on track and always be encouraging. Dan, in particular, has always made sure my committee meetings stay on topic and proceed productively. I thank my cohort for their kindness and support. I thank Annelise especially for her friendship and for embodying the type of scientist I hope to become.

I thank my partner, Kathryn for supporting me and cheering me on. Thank you for filling our apartment with adorable, amazing animals, and planning vacations to interesting places and generally encouraging me to enjoy life. I thank my parents for raising me in a loving home, providing for me, and giving me a good education. I cannot thank them enough for their hard work that allowed me to go to college debt-free. I also thank them for allowing me to seek out my own path and supporting me every step of the way.

CHAPTER 1: INTRODUCTION

Tuberculosis and *Mycobacterium tuberculosis*

Mycobacterium tuberculosis (Mtb) is a pathogenic bacteria which is the causative agent of the disease tuberculosis (TB). Mtb has co-evolved with humans for thousands of years (1) and today kills more people than any other single infectious agent (2). There were over 10 million cases of TB reported in 2017 and 1.6 million deaths, with the majority occurring in Southeast Asia and sub-Saharan Africa (2). These staggering numbers are all in the context of the development and widespread use of a TB vaccine (BCG) for almost a century, and multi-drug antibiotic therapy for over 65 years (3).

Although historically TB has affected people all over the world without regard for socioeconomic status, today it is primarily a disease of the poor, with the vast majority of new cases occurring in low-income countries (4). Poverty directly contributes to the spread of TB through factors such as crowded living conditions, inadequate diagnostic resources, as well as elevated levels of other ailments that create an elevated risk of TB (HIV, malnutrition).

The mycobacterial genus includes over 100 species that mainly consist of environmental saprophytes (organisms that live on dead/decaying organic material). Other than Mtb, the species *M. leprae*, and *M. ulcerans* are also human pathogens (5). Additionally, *M. bovis* and *M. marinum* are animal pathogens which have played a critical role in vaccine research as well as the development of animal models of Mtb infection (6, 7). Mtb and most other pathogenic Mycobacteria are characterized by an extremely slow growth rate as well as the production of complex lipids which are incorporated into the bacterial cell envelope (8).

TB is primarily a disease of the lungs, the portal of entry for infection, although the bacteria is capable of disseminating and infecting many other sites within the body (2).

Pulmonary disease generally presents with the following symptoms: cough, fever, night sweats, and weight loss. When patients present with these symptoms, they are considered to have "active TB". This is contrasted with latent TB infection (LTBI). LTBI patients have immunologic evidence of exposure to Mtb, but are asymptomatic and not contagious. For years, it has been widely believed that most, if not all, of these individuals harbor viable Mtb that is suppressed by the immune system, but have the potential to reactivate and cause active TB. However, a recent review has challenged this assumption by highlighting studies which show that most active TB develops within 1-2 years of exposure, and that true reactivation disease that occurs many years after exposure is rare (9). They argue that Mtb eradication may occur more commonly than often assumed, and that most cases of active TB in patients with "LTBI" in TB endemic regions may be due to a recent exposure rather than reactivation from an infection occurring many years ago.

Diagnosing tuberculosis

There are a number of TB diagnostics that can be used to identify infection. Sputum smear microscopy can be performed quickly and with relative ease in low-resource settings. However, this technique has limited sensitivity and cannot distinguish between different mycobacterial species (which can be prevalent in the environment) (10). The WHO recommends that initial diagnosis be confirmed with a molecular test, such as the GeneXpert MTB/RIF, whereby nucleic acid sequences specific to Mtb are amplified and detected (11). This test has high sensitivity, high specificity and can even provide information about bacterial drug resistance. Unsurprisingly, it is also much more expensive, which makes deployment in the low-resource settings where TB is prevalent more difficult (12). Another important, but slow, diagnostic is liquid culture, which also allows for drug resistance testing. All of the above

described diagnostics rely on the detection of the bacteria itself and are thus used to diagnose active TB. Another type of test can be used to detect whether individuals have been exposed to Mtb bacteria by measuring the host immune response. This test, QuantiFERON-TB Gold (QFT), involves combining host immune cells with Mtb antigens and measuring whether this results in IFN-γ production by T cells (13). Because this test does not measure the bacteria, it is restricted to identifying individuals who have been infected in the past and who either may, or may not, continue to harbor the bacteria in their bodies. Although individuals with a positive QFT test are often said to have LTBI, the proportion that actually harbor viable Mtb in their bodies is controversial. The current convention is to define LTBI as patients who test positive for QFT but from whom live bacteria cannot be cultured. While these diagnostic differences between active and latent TB appear clear cut, TB exposure may exist on a spectrum (14). Part of the trouble with defining TB exposure relates to the difficulty in accessing the primary site of infection (the lung). Thus, some tests, like the QFT, monitor a peripheral site (blood) as a proxy for the lung. While this is capable of measuring the presence of adaptive immune cells which can recognize Mtb, thus confirming prior exposure, it is much harder to assess if there are live bacteria (and if so, how many) in the lung. Although there has been some success in predicting risk of TB progression by assessing transcriptional profiles from whole blood (15), antibody responses, which are quite useful in the context of other disease diagnostics, have had more limited success, although a recent paper indicates that there may be structural differences in the antibodies of certain patient groups (16).

The BCG vaccine

BCG, the sole TB vaccine currently approved for human administration, was developed nearly a century ago by Albert Calmette and Camille Guerin in France. The vaccine consists of a live, attenuated version of *M. bovis* (17). This attenuation was achieved by passaging the bacteria *in vitro* for over a decade until key virulence properties were lost (18). The idea of inducing protection from disease by inoculating individuals with a related pathogen was linked to the earlier development of the smallpox vaccine from the related cowpox virus. To this day, BCG is administered at birth in much of the world (2). Unfortunately, the protection from TB provided by BCG is wildly variable. TB infection in infants and young children is often disseminated (occurring throughout the body), while most immunocompetent adults have disease that is largely restricted to the lungs. While BCG is quite effective at preventing disseminated disease, commonly seen in young children, its ability to confer protection against adult lung disease is more variable. Some studies have demonstrated up to 80% protection, while others have shown absolutely no protection (19). One factor that may explain this variability is geographic location as there is a correlation between the degree of protection and global latitude. This could relate to the exposure to nontuberculous mycobacteria, which are more prevalent in tropical regions where BCG protection tends to be poor (20, 21). Additionally, BCG has been hijacked as a cancer therapeutic due to its potent immunogenicity and has had particular success in the treatment of bladder cancer (22). This heterologous use of BCG also extends beyond cancer, as clinical trials have demonstrated non-specific effects of BCG which reduce childhood mortality (23), an effect that has been postulated to be due to the ability of BCG to induce "trained innate immunity" (24, 25). Because BCG immunization reduces childhood mortality broadly, beyond the protection it confers against Mtb infection, most experts believe that BCG will remain a

component of the vaccine regimen against TB (26). Indeed, many of the current TB vaccine candidates are designed as boosters on top of prior BCG immunization. The goal is that a new vaccine would prevent TB transmission. Recently, a phase II trial was conducted with an adjuvanted subunit vaccine: M72/ASO1e, in LTBI adults (27). This vaccine had 54% efficacy in preventing active TB, and importantly, most of the trial participants had previously been BCG vaccinated.

Therapeutics for tuberculosis

The development of TB therapeutics began in 1944 when two mycobactericidal antibiotics were discovered: streptomycin and para-aminosalicylic acid (PAS) (28). Unfortunately, drug resistant Mtb were already emerging in the first clinical trial for streptomycin, while dual therapy was more successful (29, 30). In addition to drug resistance, the length of treatment was initially quite long at 2 years. Over the decades, new therapeutics have been discovered and added to the regimen, and clinical trials testing treatment length have resulted in shorter treatment. Today, the WHO recommends a 6 month treatment for drug susceptible TB with 4 frontline drugs: INH, rifampin, prazinamide, and ethambutol (31). Due to the requirement for 6 months of treatment, adherence can be difficult to maintain. This can be especially problematic if patients begin to feel better due to the effects of the treatment and exhibit poor adherence. In this case, it is possible that live Mtb remain in the body and could lead to the development of drug resistance. Drug resistant TB cases are on the rise, as 30% of individuals treated in 2017 had rifampin-resistant TB (2). The treatment of drug resistant TB requires additional drugs for an even longer time.

The host immune response to Mtb infection

Mtb infection is initiated when aerosolized water droplets containing Mtb from a person with active TB are coughed up and inhaled by another person (14). These Mtb-containing droplets travel down the airway until they reach terminal alveoli, the small round air sacks which facilitate gas exchange. This anatomical site is home to alveolar macrophages (AM), a tissue resident phagocyte that is important in the surveillance of the lung mucosal barrier (32). AM develop from embryonic yolk sac-derived cells that seed the lung soon after birth (33). At steady state, this population is maintained *in situ*, although in some situations blood monocytes can contribute to the AM pool (34). These cells play a maintenance role in the alveolar space in part by metabolizing surfactant proteins (35). The importance of this is exemplified by the rare disease pulmonary alveolar proteinosis, whereby surfactant is not properly turned over and builds up (36). This is caused by dysregulation in GM-CSF production, an important AM survival signal (37). Given their positioning in the lung, AM act as the first immune cell to encounter inhaled particles and pathogens. While AM have been shown to play a protective, anti-inflammatory role in the context of some bacterial infection models (38, 39), their importance during viral infection is less clear. Depletion of AM has been demonstrated to improve the response to human metapneumovirus, while worsening the response to respiratory syncytial virus or influenza (40, 41). In addition, AM may also be important during allergic asthma (42). Due to the positioning of AM at both a location of critical importance to lung function and a site of pathogen invasion, this cell must balance the ability to initiate a sufficient immune response during infection, but also restrained enough to minimize organ damage. This balancing act is reflected in the broad array of both activating (TLR4, TNFR, IFNGR) and inhibitory (IL-10R,

TGFβR, CD200R) cell surface receptors expressed by the AM (32). Another unique feature of the AM is its use of lipid metabolism. This cell type highly expresses the transcription factor PPARγ, which coordinates the expression of genes involved in the metabolism of lipids (43). The importance of this transcription factor is highlighted by a report that macrophage-specific deletion of PPARγ leads to spontaneous lung inflammation (44). In addition, these mice also cannot control lung bacterial infection, lending evidence to the idea that PPARγ is critical in imbuing AM with the proper functions in the lung. Although it has long been assumed that AM are the first cell type to be targeted for Mtb infection, this has only recently been demonstrated experimentally (45). Here, AM were seen to be the predominant infected cell type for the first 2 weeks of infection. During this time, the infected AM relocalize from the alveolar space to the lung interstitium, which represents a critical step in the spread of bacteria to other phagocytes that reside or are recruited here. Other studies have demonstrated that AM may be a permissive cell type for Mtb replication when compared to other types of macrophages (46). In support of this, a recent, detailed transcriptional time course of infected AM revealed a surprising paucity of proinflammatory response programs (47).

Following infected AM relocalization, one of the next cell types that becomes infected are neutrophils (PMN). PMN are continually produced in the bone marrow and circulate through the vasculature, waiting for signals that could call them in to an inflamed tissue site. In addition, PMN also seem to marginate in the lung vasculature in a CXCR4-dependent manner (48), which may allow them to rapidly respond. The precise role of PMN during infection remains debated. While some groups have shown PMN to be capable of killing Mtb, others have not observed this effect, or even find them to be pathogenic (49-52). This is likely due in part to the short-lived nature of this cell type, as well as the simple correlation between level of lung inflammation and

PMN recruitment. The recruitment of PMN to the lung typically doesn't begin until D10 post-infection, which may relate, as discussed above, to the failure of infected AM to produce pro-inflammatory chemokines during the earliest stages of infection (53)

As Mtb infection proceeds, another prominent infected cell type is monocyte-derived phagocytes. These cells are recruited to the inflamed lung in large quantities during the second week of infection and by 3 weeks post-infection there are more infected PMN and monocytes than AM (45). The precise identity of these cells remains an area of active investigation. Earlier reports classified many of these cells as dendritic cells (DC) based on high expression of CD11c and CD11b (54). However, more recent work using CD64, a marker of monocyte-derived cells, supports that many of these cells are monocyte-derived (45, 55). To further complicate matters, it is also possible that conventional DC could upregulate CD64 in the context of IFNγ exposure (56). Future studies using lineage tracing reporter mice may help to shed light on these conflicting reports. In addition, studies in the zebrafish model of mycobacterial infection have found that the tissue resident macrophages are more protective, while the bacteria actively engage in the recruitment of permissive monocytes in which they can better survive (57, 58). These studies conflict with a more recent report in the mouse model, which argues that AM are more permissive than recruited macrophages, however, these discrepancies could, in part, be attributed to the adaptive immune system, which is present only in the latter model (T cells have not yet developed in zebrafish embryos used in these studies). These monocytes also seem to play a critical role in initiating the T cell response as is discussed below (59).

How do any of these phagocytes combat the bacterial infection? Mtb infects new targets by being phagocytosed. This process can be mediated by multiple different cell surface molecules including mannose and complement receptors (60). Following phagocytosis, there are

a number of different outcomes that can occur which depend both on the state of the host cell as well as the bacteria. Phagosomal maturation, whereby fusion occurs between multiple phagosomal and lysosomal vesicles in order to modify the membrane proteins and contents of the vesicle can eventually lead to this becoming a hostile environment through the lowering of the pH and activation of pH-sensitive degradation enzymes. However, Mtb has a number of mechanisms in place which can inhibit this process and maintain the phagosome as a hospitable environment. This blockade of phagosomal maturation occurs through interactions between bacterial cell surface features (ManLAM) or secreted proteins (SapM) and host proteins (PIP3) (61-63). In addition, yet other bacterial products (PtpA) seem to play a role in preventing the phagosome from acquiring the V-ATPase proton pump, which facilitates compartment acidification (64). It is also possible for Mtb to induce damage to the phagosomal membrane and thus escape into the cytosol. This process is dependent on the type 7 bacterial secretion system ESX-1 as well as the lipid PDIM (65-67). The implications of cytosolic Mtb localization remain confusing. It has been demonstrated that Mtb can be sensed by the cGAS-STING pathway, resulting in the production of type I IFN (68-70). This may actually be beneficial to the bacteria, as type I IFN signaling, especially in highly susceptible mouse models of Mtb, results in increased mortality (71). On the other hand, cytosolic Mtb can also be targeted to the autophagosome through TBK1 (72).

The adaptive immune response, and in particular CD4 T cells, have long been known to be required for protection from Mtb. The importance of CD4 T cells is best illustrated by the situation of HIV/Mtb coinfection. Here, HIV targets and depletes CD4 T cells, and this results in increased susceptibility to TB (73). In the mouse model, loss of CD4 T cells leads to rapid mortality when compared to loss of CD8 T cells or B cells (74). Despite the importance of CD4

T cells, there are a number of barriers which seem to limit their effectiveness at controlling infection. The initiation of the T cell response to Mtb is delayed when compared to other infections (75). In order for Mtb-specific T cells to be primed and recruited to the lung, live Mtb must be transported to the lung-draining LN which does not occur until after 1 week of infection. T cells do not appear in the lung for at least another week (76, 77). This is consistent with human studies where a detectable immune response to Mtb is typically not observed until over 1 month after exposure (78, 79). Another aspect that restricts CD4-mediated immunity is the concurrent expansion of Mtb-specific regulatory T cells (Tregs). While Tregs are best appreciated for their important role in restraining autoimmune disease, here their recognition of the pathogen is problematic. These cells recognize Mtb antigens and are activated in the LN with similar kinetics to effector CD4s and suppress a potentially more robust antibacterial immune response (80). Interestingly, the activation of these Tregs is context specific and is not observed in Mtb antigen-expressing Listeria (81). These early roadblocks in getting effector T cells to the lung give the bacteria extra time to set up an immunosuppressive niche that limits the functionality of the immune cells once they do finally arrive. This has led to the idea that if T cells could be positioned in the lung prior to this remodeling, perhaps they could be more protective.

Once T cells arrive in the lung, how do they curb the pathogen? The development of a Th1 response has long been associated with protection, as genetic knockouts of the Th1 cytokine IFN-γ as well as factors required for the development and maintenance of Th1s (IL-12, T-bet) are highly susceptible to infection (74). More recently, other CD4 cytokines such as IL-17 have also been implicated in control in the context of vaccination (82). Finally, a report last year showed that a TNF superfamily molecule, CD153, also seems to be important for the protection conferred by CD4 T cells (83). Regardless of the effector molecules they produce and their

ability to home to the site of infection, CD4 T cells are incapable of inducing sterilizing immunity to Mtb in animal models. Thus, the infection continues chronically. This leads to accumulation of lung damage and eventual mortality. The chronic stage of infection provides new problems for the T cell response. Much like in the chronic disease of cancer, where CD8 T cells become exhausted due to persistent antigen stimulation (84), so too does a similar process occur with Mtb-specific CD4s. This has been demonstrated in both mice and humans whereby an immunodominant Mtb antigen that is expressed throughout infection leads to terminal differentiation of CD4 T cells and impaired cytokine production (85).

Dissertation objectives and significance

Given the chronic nature of Mtb infection, as well as the abundance of both *in vivo* and *in vitro* systems for probing host-pathogen interactions, there is a significant body of work concerning the features of the CD4 T cell response during infection *in vivo*, and factors important for phagocyte control of Mtb *in vitro*. However, less is known about the very early events of infection and the impact of the spread of Mtb to different host cell types. This is likely due in part to the difficult in accurately measuring the features of early immunity. Despite the challenges presented, a better understanding of this early stage of infection is highly relevant to the development of vaccines given evidence that the immune events that occur early likely have a large impact on the course of chronic infection. In addition, there are a variety of different cell types which are temporally targeted for infection. Evidence both from TB as well as other diseases have demonstrated that cell-type specific differences exist which could dictate differential control depending on what type of phagocyte engulfs Mtb. Thus, the major goal of

this work is to characterize the dynamics and immune responses of T cells and infected phagocytes during early Mtb infection.

One arm of this work relates to the delayed recruitment of CD4 T cells to the lung. This has led to the idea that if T cells could simply reach the lung earlier, prior to the development of an immunosuppressive niche, then perhaps these cells could be more effective. This goal has been pursued in the design of new vaccines. Thus, we have engaged in studies to position T cells in the lung early during infection to monitor their protective capacity. Here we found that T cells could only provide protection once Mtb resided in lung-recruited monocyte-derived macrophages. This cell type engages multiple proinflammatory signaling pathways compared to alveolar macrophages, which are less inflammatory, and less protective. This will be discussed in Chapter 3.

A second arm of this work relates to how prior vaccination affects early immunity to Mtb. There is still much we do not understand about how BCG, the only approved TB vaccine, modulates immunity to Mtb. Here, we found that BCG mediates the accelerated transfer of infection from alveolar macrophages to lung-recruited phagocytes in a CD4 T cell-dependent process. In addition, this transfer precedes vaccine-induced protection, which only occurs after T cells colocalize with the infectious lesion. These findings, discussed in Chapter 4, have significant implications for future vaccine strategies.

CHAPTER 2: MATERIALS AND METHODS

Mice

ESAT-6 TCRtg (C7) mice were provided by Eric Pamer and have been described previously (86). OT-II mice were provided by Michael Gerner (University of Washington). LRRK2$^{-/-}$ mice were provided by Huaibin Cai (NIH). C57BL/6, MHCII$^{-/-}$, and NOS2$^{-/-}$ mice were purchased from Jackson Laboratories (Bar Harbor, ME). All mice were housed in specific pathogen-free conditions at Seattle Children's Research Institute (SCRI). Experiments were performed in compliance with the SCRI Animal Care and Use Committee. Both male and female mice between the ages of 8-12 weeks were used.

BCG immunization

BCG-Pasteur was cultured in Middlebrook 7H9 broth at 37°C to an OD of 0.2-0.5. Bacteria was diluted in PBS and 10^6 CFU in 200ul was injected subcutaneously. After immunization, mice were rested for 8 weeks prior to Mtb infection.

Aerosol Infection and CFU enumeration

Infections were performed with wildtype H37Rv Mtb or H37Rv transformed with an mCherry or Wasabi reporter plasmid (87). Mice were enclosed in a Glas-Col inhalation exposure system and 50-100 CFU were deposited directly into the lungs. To determine Mtb CFUs, lungs were homogenized in 0.05% Tween 80 in PBS. Ten-fold serial dilutions were made in 0.05% Tween 80 and plated on 7H10 plates. Colonies were counted after 21 days of incubation at 37°C.

Intratracheal and intravenous antibody labeling

For intratracheal (i.t.) labeling, 30min prior to sacrifice, mice were anesthetized with 20% isoflurane in propylene glycol (Fisher Scientific) and 0.25ug of CD45.2 PE-Cy7 in 50ul of PBS was pipetted into the airway. For intravenous (i.v.) labeling, mice were anesthetized as above and infused with CD45.2 PE 10 min prior to sacrifice.

Lung cell isolation and antibody staining

Mouse lungs were homogenized in HEPES buffer with Liberase Blendzyme 3 (70ug/ml; Roche) and DNaseI (30ug/ml; Sigma-Aldrich) using a gentleMacs dissociator (Miltenyi Biotec). Lungs were incubated at 37°C for 30 min and then further homogenized with the gentleMacs. Cells were filtered through a 70um cell strainer and resuspended in RBC lysis buffer (Thermo) prior to a PBS wash. Cells were next incubated with 50ul Zombie Aqua viability dye (BioLegend) for 10min at room temperature (RT). Viability dye was quenched with 100ul of antibody cocktail in 50% FACS buffer (PBS containing 2.5% FBS and 0.1% NaN3)/50% Fc block buffer. Staining was performed for 20min at 4°C. Cells were washed with FACS buffer and fixed with 2% paraformaldehyde for 1hr prior to analysis on an LSRII flow cytometer (BD Biosciences). When stain sets contained tetramers, staining was performed for 1hr at RT. Ag85B (I-A(b) 280-294) and TB10.4 (K(b) 4-11) tetramers were obtained from the NIH Tetramer Core Facility. Intracellular phospho-S6 (Ser235/236 2F9; Cell Signaling), phospho-STAT1 (Tyr701 C14; BD Biosciences), and NOS2 (CXNFT; Thermo Fisher) staining was performed for 1hr at RT with the FoxP3/Transcription Factor Staining Kit (Invitrogen). To measure mitochondrial membrane potential, cells were incubated with TMRM (Thermo Fisher) for 30min at 37°C prior to antibody staining.

BrdU proliferation analysis

2mg of BrdU was injected i.p. into previously infected mice 1d prior to sacrifice. BrdU was detected by flow cytometry using the BD BrdU Flow Kit (BD Biosciences).

Deconvolution microscopy

Lung cells from mCherry infected mice were isolated and antibody stained as described above. Macrophage populations were sorted on a cell sorter (FACSAria, BD Biosciences) directly into 2% PFA. A Cytospin (Thermo Fisher) was used to transfer sorted cells onto slides, which were then coverslipped with DAPI-containing mounting media (ProLong Diamond; Thermo Fisher). Imaging was performed using a Deltavision Elite microscope (GE Life Sciences). Deconvolution was performed with SoftWoRX (GE Life Sciences) and image analysis was performed with Fiji (NIH).

Confocal Microscopy

Mice were infected with H37Rv Mtb-mCherry and sacrificed at D10 and D14. Lungs were excised and submerged in BD Cytofix fixative solution diluted 1:3 with PBS for 24hr at 4°C. Lungs were washed 2x in PBS and dehydrated in 30% sucrose for 24hr prior to OCT embedding and rapid freezing in a methylbutane-dry ice slurry. 20um sections were stained overnight at RT (with the following antibodies: CD11c BV480; HL3 (BD), CD11b BV510; M1/70 (BD), CD45.2 AF700; 104 (BioLegend), MHC-II APC-Fire750; M5/114.15.2 (BioLegend), Siglec-F BV421; E50-2440 (BD), pS6 AF488; 2F9 (Cell Signaling), CD3 CF633; 17A2, CD4 CF660C; RM4-5) and coverslipped with Fluoromount G mounting media (Southern Biotec). Images were acquired

on a Leica SP8X confocal microscope, compensated for fluorophore spillover using LAS X (Leica), and analyzed with Imaris (Bitplane) and FlowJo as previously described (88).

T cell depletion and FTY720 treatment

To deplete T cells, mice were intraperitoneally (i.p.) injected with 400ug anti-CD4 GK1.5 or anti-CD8 2.43 (BioXcell) in PBS at D-1, D4, and D10 relative to infection. To block T cell egress, mice were i.p. injected with 1mg/kg FTY720 (Sigma) in water daily starting 2d prior to harvest.

IFN-γ treatment

Mice were anesthetized with 20% isoflurane in propylene glycol (Fisher Scientific) and 1ug of purified IFN-γ (PeproTech) was delivered i.t. in 50ul PBS.

Bone marrow chimeras

To create mixed MHCII$^{-/-}$ chimeras, WT CD45.1/2 F1 mice were irradiated with 1000 rads and reconstituted with a 1:1 mixture of CD3-depleted (Miltenyi Biotec) CD45.1 B6.SJL:CD45.2 MHCII$^{-/-}$ bone marrow ($7x10^6$ cells/mouse). At D56 post-reconstitution, mice were immunized with BCG. To create mixed NOS2$^{-/-}$, WT CD45.1 B6.SJL mice were irradiated with 1000 rads and reconstituted with a 1:1 mixture of CD3-depleted (Miltenyi Biotec) CD45.1/2 F1:CD45.2 NOS2$^{-/-}$ bone marrow. To create criss-cross NOS2 chimeras, host mice were irradiated as above and reconstituted with $5x10^6$ donor cells. WT B6 mice were reconstituted with WT CD45.1/2 F1 cells. NOS2$^{-/-}$ mice were reconstituted with either NOS2$^{-/-}$ or WT CD45.1/2 F1 cells. WT CD45.1 B6.SJL mice were reconstituted with NOS2$^{-/-}$ cells.

Th1 polarization and adoptive transfers

CD4 T cells from ESAT-6-specific (C7) CD90.1+ and OVA-specific (OTII) CD45.1+ TCR transgenic mice were negatively enriched from spleens using EasySep magnetic microbeads (STEMCELL). T cells were Th1 polarized as follows: 1.6 × 106 transgenic T cells were cultured with 8.3 × 106 irradiated CD3- splenocytes. 5 μg/ml of ESAT-6 or OVA peptide, 10 ng/ml IL-12, and 10 μg/ml of anti–IL-4 antibody (R&D Systems) were added at D0. At D3, cells were split 1:2, and 10 ng/ml IL-12 was added (R&D Systems). On D5, Th1 cells were delivered i.v. or i.t. into mice.

RNA sequencing and transcriptional analysis

For host sequencing, macrophage populations were sorted from mCherry-infected mice and resuspended in TRIzol (Thermo Fisher). RNA isolation was performed by phenol-chloroform extraction and cDNA library preparation was done with the SMART-Seq v4 Ultra Low Input RNA Kit (Takara). Sequencing was performed at the Institute for Systems Biology (ISB) (Seattle, WA) and analyzed using DESeq2 (89). Transcription factor binding analysis was performed with the cMonkey2 package (90).

Mtb sequencing was performed as described in a recent publication (91). After cDNA preparation, libraries were enriched for Mtb transcripts using biotinylated, Mtb-specific oligonucleotides and subsequent capture with magnetic streptavidin beads. Library amplification was performed with SureSelectXT (Agilent). Sequencing was performed at ISB and analyzed using the following tools: RoundRobin, RankProduct (92), SAM (93), EdgeR (94), and DESeq2 (89) .

Data acquisition and analysis

Flow cytometry data were analyzed using FlowJo V10 software (Tree Star) and presented as means ± SEM. Statistical analysis and graphical representation of data were done using GraphPad Prism v6.0 software. At least 3-5 mice were used per group in each experiment, as indicated in figure legends, and all experiments were performed at least 2 times. Statistical significance was determined using a t-test or ANOVA.

CHAPTER 3: Alveolar and monocyte-derived macrophages differentially engage antibacterial response programs

Introduction

The requirement for a robust CD4 T cell response during Mtb infection has been demonstrated many times over. Knockout mice lacking CD4 or various CD4 T cell effector genes are highly susceptible to Mtb infection (74). In addition, HIV-infected individuals with depressed levels of CD4 T cells have an elevated risk of TB (73). Thus, a major effort of TB vaccine development has been to boost the CD4 T cell response, with the idea that this might lead to enhanced protection. In 2013, a clinical trial was conducted with MVA85A, a viral-based TB vaccine (95). This was a first trial of a new TB vaccine since BCG. This vaccine was able to confer a significant boost in the production of multiple cytokines by CD4 T cells. However, unfortunately, MVA85A provided absolutely no additional protection over BCG alone. While there are a number of potential explanations for this failure, one interesting component of the T cell response which could play a role here has to do with T cell localization. Given that the primary site of Mtb infection is the lungs, it is critical that T cells reach this site of infection. This is not a trivial task given that, as is discussed in the introduction, there are a number of barriers that hinder the rapid, effective response of T cells in the lung. In the MVA85A trial, T cell responses were assessed in peripheral blood, thus it remains unclear if the changes in cytokine production observed here were also reflective of changes in T cells in the lung. This is further complicated by the fact that, more recently, it has been demonstrated that overproduction of IFN-γ by CD4 T cells can be detrimental, leading to increased immunopathology in the lung and ultimately, more rapid mortality (96).

To address whether boosting the number of cytokine-producing CD4 T cells in the lung could confer protection, Gallegos et al., created and adoptively transferred transgenic Mtb-

specific Th1 cells intravascularly (i.v.) 1 day prior to aerosol Mtb challenge (86). Surprisingly, even large numbers of adoptively transferred Mtb-specific Th1 cells (~10^7) had no effect on the lung bacterial burden during the first week after aerosol infection, but only led to reduced bacterial burdens thereafter. Since this publication, it has become clear that only a subset of the T cells recovered from enzyme-digest lung cell suspensions represent cells that actually reside in the lung parenchyma, whereas others represent T cells resident in the lung vasculature. T cells residing in each of these locations can be distinguished by using an i.v.-administered antibody label immediately before euthanasia (97). Using this approach, our lab and others have shown that T cells resident in the lung parenchyma re-traffic rapidly to the lung parenchyma upon adoptive transfer and reduce the lung bacterial burden, whereas those in the vasculature do not traffic into the lung and provide little or no protection (98, 99). Because the prior study had not used i.v.-labeling, this raised the possibility that the i.v. transferred T cells were not protective because they did not efficiently traffic to the site of infection within the lung parenchyma and remained in the lung vasculature. Thus, we sought to re-visit these experiments, to determine whether T cells that do traffic to the lung parenchyma may indeed be able to confer protection during the first week after aerosol infection.

Results

To understand whether Mtb-specific CD4 T cells can mediate early protection, we first repeated the i.v adoptive transfers, as previously performed by Gallegos et al. (86). In order to define the localization of these cells within the lung, we utilized both an i.v. as well as an airway antibody label (Fig. 1A-B). Similar to the previous report, we also observed that the i.v. transfer did not confer protection 7 days post-infection (Fig. 1C). When we assessed the localization of

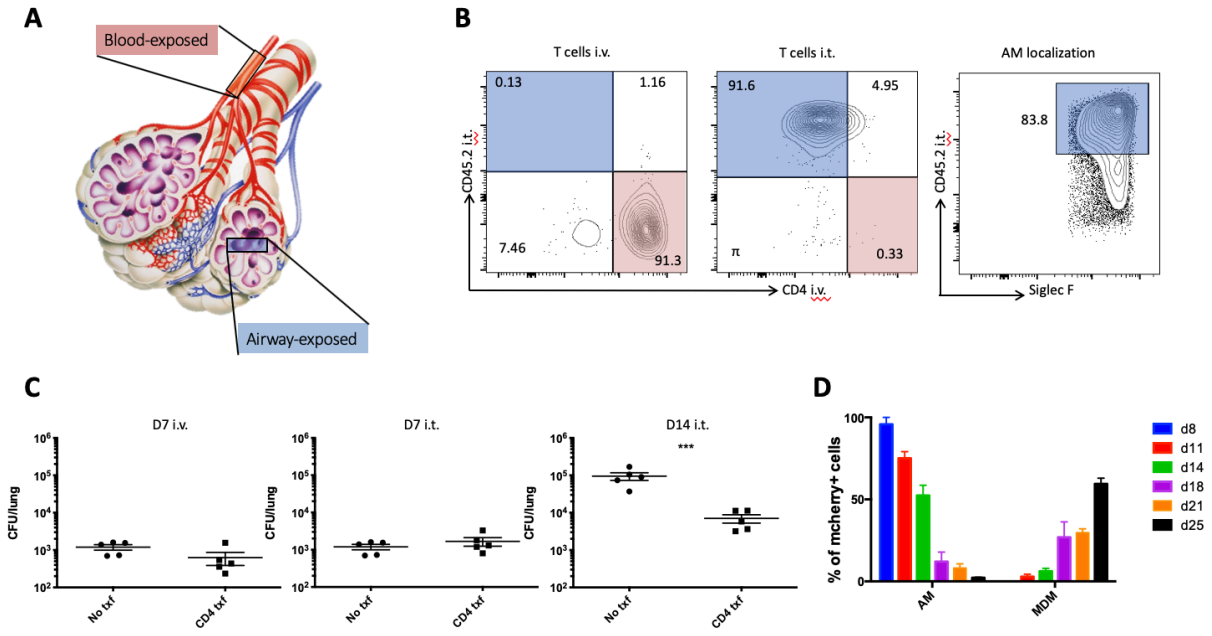

Figure 1: Adoptively transferred Th1 cells provide delayed protection.
(A) Graphic depicting how the use of i.v. and i.t. antibody labeling distinguishes the lung vasculature (blood-exposed) and the lung airway (airway-exposed). (B) Representative flow plots of adoptively transferred T cells (gated on $CD3^+$ $CD4^+$ $CD90.1^+$) and AM (gated on $Siglec\text{-}F^+$ $CD11c^+$) from the lungs of mice infected 1d prior. (C) Lung bacterial burdens of mice that did or did not receive adoptive T cell transfers at D7 and D14 post-infection. (n=5 mice/group). (D) Composition of $mCherry^+$ lung cells (AM: $CD11c^+$ $Siglec\text{-}F^+$, PMN: $CD11b^+$ $Ly6G^+$, MDM: $CD11b^+$ $CD64^+$) at D14 as determined by flow cytometry (n=5 mice/group) This panel is adapted from Cohen et al. Single-group comparisons were performed by unpaired t test. Data are presented as mean ± SEM. ***$p < 0.001$. All experiments were performed at least 2–3 times.

these T cells, however, the vast majority resided in the lung vasculature rather than the lung parenchyma. This is important because alveolar macrophages (AM), the first cell type to become infected with Mtb, are located in the alveoli and readily label with the airway antibody label (Fig. 1B). Thus, the transferred T cells are not in the correct location to directly interact with infected AM and mediate protection. We next performed similar adoptive transfers but with a different route of administration. Here we delivered T cells directly into the airways of deeply anesthetized mice prior to Mtb infection the next day. Although we confirmed that these T cells were transferred into the airways, and subsequently migrated into the interstitium, we were surprised to find that these transfers were also unable to provide any protection during the first

week of infection. In fact, similar to as was reported in the i.v. transfer experiments (86), we were able to observe protection only after 2 weeks of infection (Fig. 1C). Given that our airway transfers seemed to correctly position CD4 T cells to interact early with infected macrophages, we next considered what else could be responsible for this delay in protection. Our lab and others have previously shown that, as infection proceeds, different types and proportions of phagocytes become infected over time (45, 54). When we performed a time course using a fluorescently labeled strain of Mtb to track the infected cell types, we found that AM were the predominant infected cell type 1 week post infection, and remained the major infected cell type until D14 (Fig. 1D). After this time point, we began to detect significant proportions of infected lung-infiltrating monocyte-derived macrophages (MDM) and neutrophils (PMN). Thus, the later time point when the T cell transfers provide protection seemed to correlate with the decrease in infected AM and the increase in other infected phagocytes. Given that it has previously been demonstrated that different phagocytes as well as their activation state, can profoundly affect their ability to restrict Mtb growth (46, 57, 58) we hypothesized that perhaps infected AM poorly control Mtb, even in the face of CD4 T cell help.

To begin to address the protective capacity of different macrophage populations, we focused on AM and MDM given that these cell types are the major infected cell type early and later post-infection respectively. We performed a time course wherein we infected animals with fluorescent, mCherry-expressing Mtb, and then sorted out infected AM and MDM in order to perform imaging and quantify the bacterial burden on a per cell basis (Fig. 2). At D14 post infection, we found that there were significantly more bacteria in AM compared to MDM. In addition, the number of bacilli in AM ranged from 1 to 30 (median=8) compared to 1 to 12 for MDM (median=1). However, this single time point could reflect the fact that the bacteria have

more recently infected the MDM and have had less time to replicate, while the bacteria in AM have replicated more because they have been in that cell type for longer. Counter to this

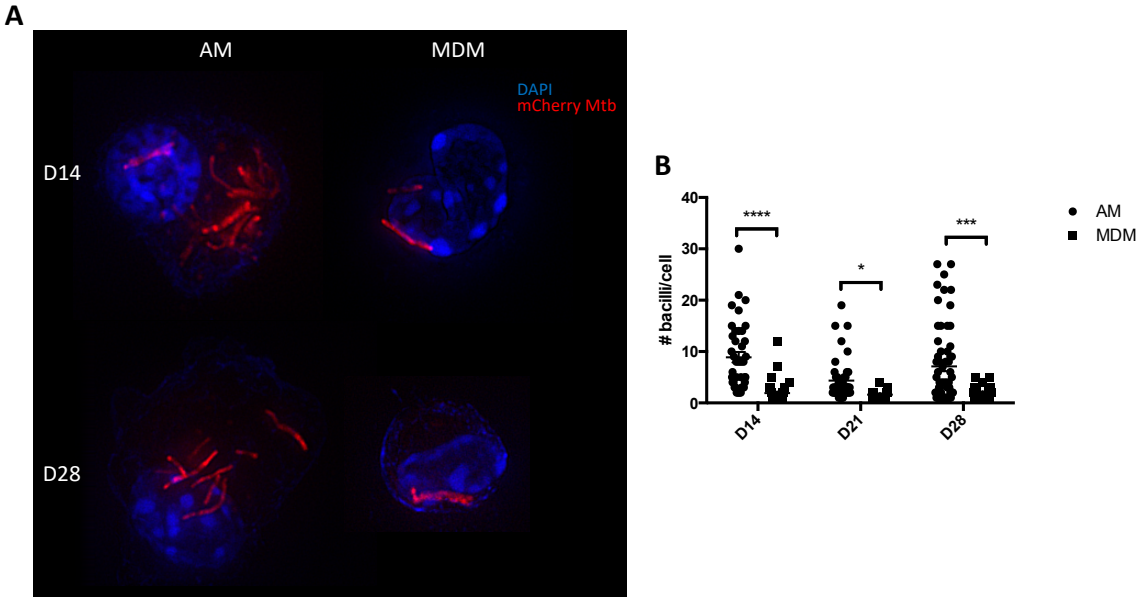

Figure 2: AM harbor more bacteria than MDM.
(A) Representative fluorescence images of infected AM and MDM sorted from mCherry-Mtb infected mice at D14 and D28. (B) Quantification of the number of Mtb bacilli per cell in AM and MDM at D14, D21, and D28 (n=18-49 cells/group/timepoint). Single-group comparisons were performed by unpaired t test. Data are presented as mean ± SEM. *$p < 0.05$, ***$p < 0.001$, ****$p < 0.0001$. All experiments were performed at least 2–3 times.

argument, when we performed imaging analysis of infected cells recovered from D21 and D28 post infection, these patterns of higher average number of bacteria per cell in AM and larger range in AM continued to hold. From these data, it seems that MDM may be innately more capable of restricting bacteria growth compared to AM. In addition, given that D28 is the height of the T cell response, and it is known that the overall lung bacterial burden has leveled off by this time point, the fact that AM still retain more bacteria supports that control of Mtb by this cell type does not seem to be significantly aided by adaptive immunity.

Why do AM harbor high levels of bacteria even after Mtb-specific CD4 T cells have been recruited to the lung? It has previously been demonstrated that cognate interactions between CD4

T cells and infected macrophages are required for optimal control (100). Thus, we considered the possibility that either AM do not express the proper receptors to facilitate T cell interactions, or AM are not responsive to T cell cytokines. To investigate the first possibility, we performed surface staining for MHCII, as well as the costimulatory markers CD80 and CD86 (Fig. 3).

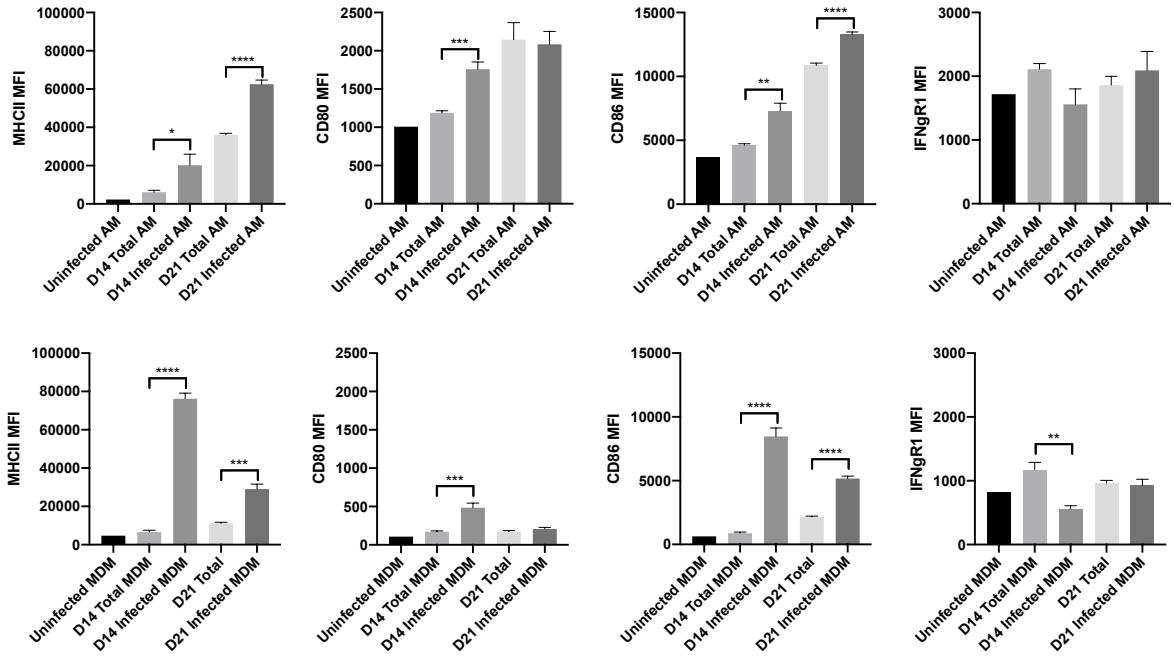

Figure 3: AM and MDM similarly upregulate antigen presentation molecules.
Cell surface expression of MHCII, CD80, CD86, and IFNgR1 on AM and MDM at D14 and D21 post-infection was determined by flow cytometry. Single-group comparisons were performed by unpaired t test. Data are presented as mean ± SEM. *$p < 0.05$, **$p < 0.01$,***$p < 0.001$, ****$p < 0.0001$. All experiments were performed at least 2–3 times.

Here we found that both infected AM and infected MDM significantly upregulate MHCII at both D14 and D21 relative to uninfected cells. Similarly, CD80 was significantly upregulated in both cell types at D14, and CD86 was significantly upregulated at both time points. Thus, AM seem to express the requisite cell surface molecules to both present antigen and to deliver costimulatory signals to CD4 T cells. Next, to assess macrophage responsiveness to T cell

cytokines, we investigated the IFNγ pathway. We first stained for the ligand-binding subunit of the IFNγ receptor, IFNγR1 (Fig. 3). Although we observed slightly less express of IFNγR1 in Mtb-infected MDM than their uninfected counterparts at D14 (and a trend towards less expression in infected AM), by D21 we observed no difference in expression between infected and uninfected AM or MDM. In order to test functionally whether these macrophages were competent to respond to IFNγ, we performed intracellular staining for phosphorylated STAT1 (p-STAT1), which occurs downstream of IFNγ signaling. To understand whether lung macrophages are IFNγ-responsive at steady state, we treated uninfected animals with intratracheal IFNγ for 1 hour prior to sacrifice (Fig. 4A). Here we observed a significant increase

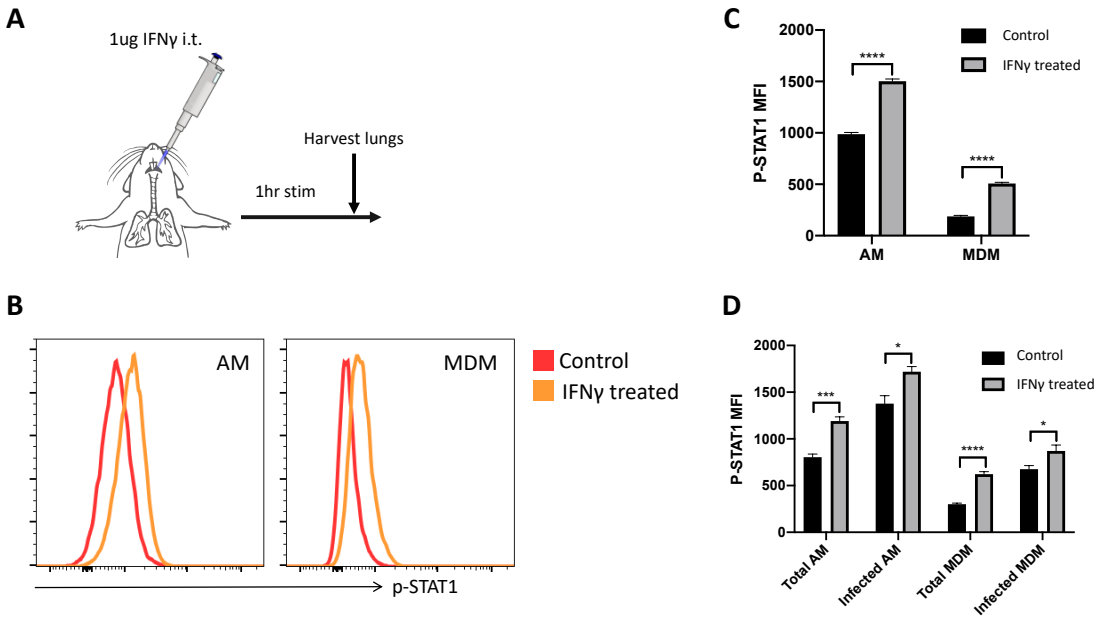

Figure 4: AM and MDM are competent for sensing IFNγ
(A) Schematic depicting the i.t. delivery of IFNγ for a 1hr *in vivo* stimulation prior to animal sacrifice. (B) Representative histograms showing p-STAT1 staining in AM and MDM from naïve animals. (C) Graph depicting the level of p-STAT1 in AM and MDM from naïve animals (n=5 mice/group). (D) Graph depicting the level of p-STAT1 in AM and MDM from D14 infected animals (n=5 mice/group). Single-group comparisons were performed by unpaired t test. Data are presented as mean ± SEM. *p < 0.05,***p < 0.001, ****p < 0.0001. All experiments were performed at least 2–3 times.

in p-STAT1 in both AM and MDM (Fig. 4B-C). To test whether Mtb infection alters this responsiveness, we performed a similar treatment at D14 post infection (Fig. 4D). At this time point, we again observed a significant increase in p-STAT1 in total AM and MDM. In addition, the p-STAT1 within untreated infected AM and MDM appeared to be higher at baseline, and significantly increased in the treated group. Based on these studies, it appears that infected AM (and MDM) are capable of responding to IFNγ. Finally, we considered that IFNγ production by T cells within the lung could be highly localized. This could lead to differential IFNγ exposure between AM and MDM. To address this, we performed serial IFNγ treatments starting at D14 and assessed the lung at D21. There were no significant differences in the cell types targeted for infection or in the lung bacterial burden (Fig. 5A-B). Additionally, we performed intracellular

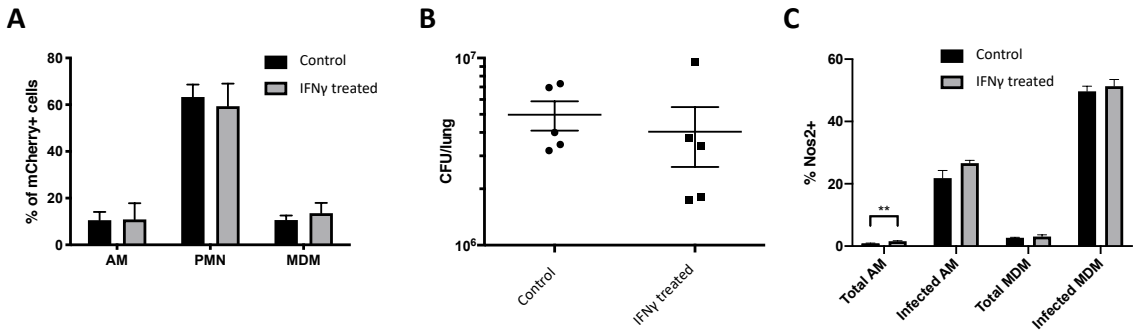

Figure 5: IFNγ supplementation does not affect early infection.
Previously infected animals were treated with 1ug i.t. IFNγ on D14, D16, and D19 prior to sacrifice on D21 (n=5 mice/group). (A) Composition of mCherry$^+$ lung cells (AM: CD11c$^+$ Siglec-F$^+$, PMN: CD11b$^+$ Ly6G$^+$, MDM: CD11b$^+$ CD64$^+$) as determined by flow cytometry. (B) Lung bacterial burden as determined by dilution plating. (C) Proportion of AM and MDM which express Nos2 as determined by flow cytometry. Single-group comparisons were performed by unpaired t test. Data are presented as mean ± SEM. **$p < 0.01$. All experiments were performed at least 2–3 times.

staining for NOS2, an IFNγ-inducible gene that is known to be important for control of Mtb (101) (Fig. 5C). While there was a small, but significant, increase in the proportion of NOS2$^+$ total AM in the treated group, this was not observed within the infected AM. There was also no

difference in the proportion of $NOS2^+$ MDM in the treated group. Thus, it does not appear that infected AM make less Nos2 due to a paucity of IFNγ.

Given that these macrophage populations seemed to differ in their protective capacity, we next set out to understand what genetic programs might be responsible for their disparate responses. We first performed RNA-seq of infected AM and MDM, as well as uninfected AM and MDM (from the same infected animals) at D14 post infection. When we performed principle component analysis (PCA), we observed that, while each of the 4 groups clustered distinctly, there seemed to be larger differences between the uninfected and infected MDM while the uninfected AM was relatively more similar to the infected AM (Fig. 6A). This was also reflected when we looked differential gene expression analysis. Here, we found that there were almost 2000 differentially expressed genes in infected MDM relative to uninfected MDM, while there were only about 250 in infected AM relative to uninfected AM (Fig. 6B). These larger differences in gene expression MDM compared to AM was surprising given the fact that the AM have likely been infected for longer, and may reflect the fact that the MDM are being called in to the infected lung through proinflammatory signals, and thus may be better primed to quickly initiate a robust cellular immune response.

In order to identify genes which could play a role in the differential response, we compared gene expression in infected AM and infected MDM. Here, we identified 9 genes which were significantly induced in one cell type, and significantly repressed in the other (Fig. 6B, Table 1). Interestingly, two of these genes, Lrrk2 and IFITM3, have been shown to play a regulatory role in phagosomal maturation (102-104). Both of these genes were significantly induced in infected AM compared to uninfected AM, while significantly repressed in MDM

(Fig. 6C). In addition, infected AM more highly expressed Lrrk2 than infected MDM. Previous reports have shown that Lrrk2 may also play a functional role during TB (105). One study used a

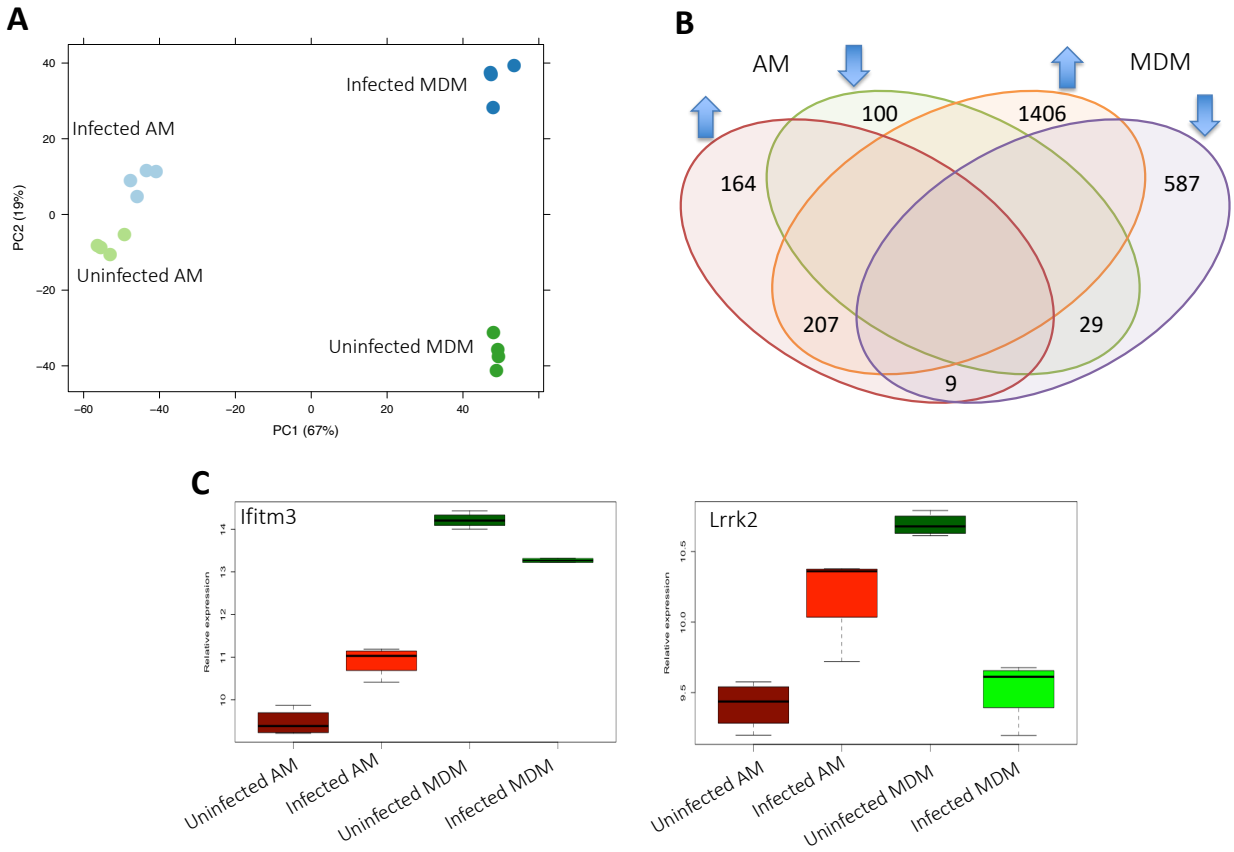

Figure 6: Transcriptional differences between AM and MDM at D14.
Infected and uninfected AM and MDM were sorted from D14 mCherry infected animals for RNA-seq (each sample was generated from the lung cells sorted from 10 pooled mice, n=4 samples/group). (A) PCA plot showing the clustering of replicates within each group. (B) Venn diagram showing the number of differentially expressed genes (log2 foldchange>1, adjusted p-value<0.05) in infected AM and MDM (relative to uninfected cells of the same group). Arrows indicate up or downregulated genes. (C) Gene expression of two differentially expressed genes with known regulatory roles in phagosome maturation.

Lrrk2 KO mouse to show that KO macrophages are better at phagolysosomal fusion, which correlates with a decreased lung bacterial burden (106). Interestingly, this decreased CFU was only observed at early time points (D7-14), while there was no difference in the CFU during chronic infection (D56). Based on this, we speculated that the transient protection during early infection could relate to derepresssion of phagolysosomal fusion specifically in AM, while at later

Gene	Description
Vnn3	involved in vitamin B5 metabolism
Pkdcc	secreted kinase, phosphorylates MMPs
Lrrk2	phagosomal regulator in the context of Mtb
Ifitm3	ISG, important during Mtb, colocalizes with phagosome, induces acidification
Hpse	heparanase, marks inflammatory monocyte/ macrophages
Hp	Haptoglobin, binds hemoglobin
Gpr141	GPCR, IFN/TNF-induced
Acer3	involved in lipid metabolism, anti-inflammatory
CD300Lg/Trem4	surface receptor, may be involved in Ab/ lymphocyte interactions

Table 1: Differentially regulated genes at D14.
List of genes which were upregulated in infected AM and downregulated in infected MDM at D14 as in Fig. 6B.

time points this is lost as MDM become the predominant bacterial target, which are more competent at phagolysosomal fusion. We hypothesized that if we were to assess the cell types targeted for infection in Lrrk2 KO animals, we would see less infected AM if the Lrrk2 KO version of these cell types are more protective. However, when we assessed the infected cell types of control and Lrrk2 KO animals at D14 post infection, we found no significant differences (Fig. 7A). In addition, the previously reported CFU phenotype was observed in an experiment in which mice were infected with a relatively high, non-physiologic aerosol Mtb dose (200 CFU), raising the possibility that the effect may be dose dependent. Consistent with this possibility, we observed no protection at a low dose (depo=20), and a trend towards protection at a higher dose infection (depo=225) (Fig. 7B). Finally, using the MFI of mCherry fluorescence as a proxy for

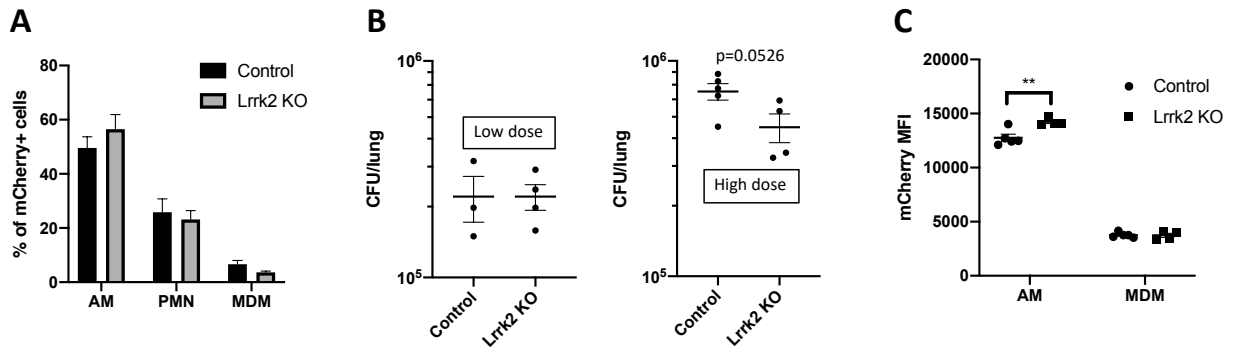

Figure 7: Loss of Lrrk2 minimally affects early Mtb infection.
WT and Lrrk2 KO animals were infected with a low (infectious dose = 20) or high (infectious dose = 225) dose of mCherry-Mtb and sacrificed at D14. (A) Proportion of mCherry$^+$ cells as determined by flow cytometry from high dose experiment. (B) Lung bacterial burdens of low and high dose infected animals. (C) Mean fluorescence intensity (MFI) of mCherry signal in AM and MDM from high dose experiment. Single-group comparisons were performed by unpaired t test. Data are presented as mean ± SEM. **$p < 0.01$. All experiments were performed at least 2–3 times.

bacterial load on a per cell basis, we did not observe that infected Lrrk2 KO AM had less bacteria (Fig. 7C). Instead, there was a small but significant increase in the mCherry in the KO. However, based on this measurement, we are unable to distinguish if all of the bacteria within the AM are alive.

We next performed similar transcriptional analyses at D20 post infection. This time point was chosen because it represents an early point following the recruitment of antigen specific CD4 T cells to the lung and thus the infected macrophages could have encountered T cells, and or been exposed to T cell cytokines. Unsurprisingly, the PCA showed that the infected MDM remain distinct from uninfected MDM (Fig. 8A). Interestingly, at this time point, the infected AM seem to be more different than uninfected AM, indicating that there may be changes in the transcriptional program of infected AM between 2 and 3 weeks post infection. This is also reflected in the similar numbers of differentially expressed genes found between both infected cell types and their uninfected counterparts (Fig. 8B). We next performed gene set enrichment analysis (GSEA) on the transcriptional data from both D14 and D20 (Fig. 8C). Through this analysis, we identified significant enrichment in multiple different proinflammatory signaling

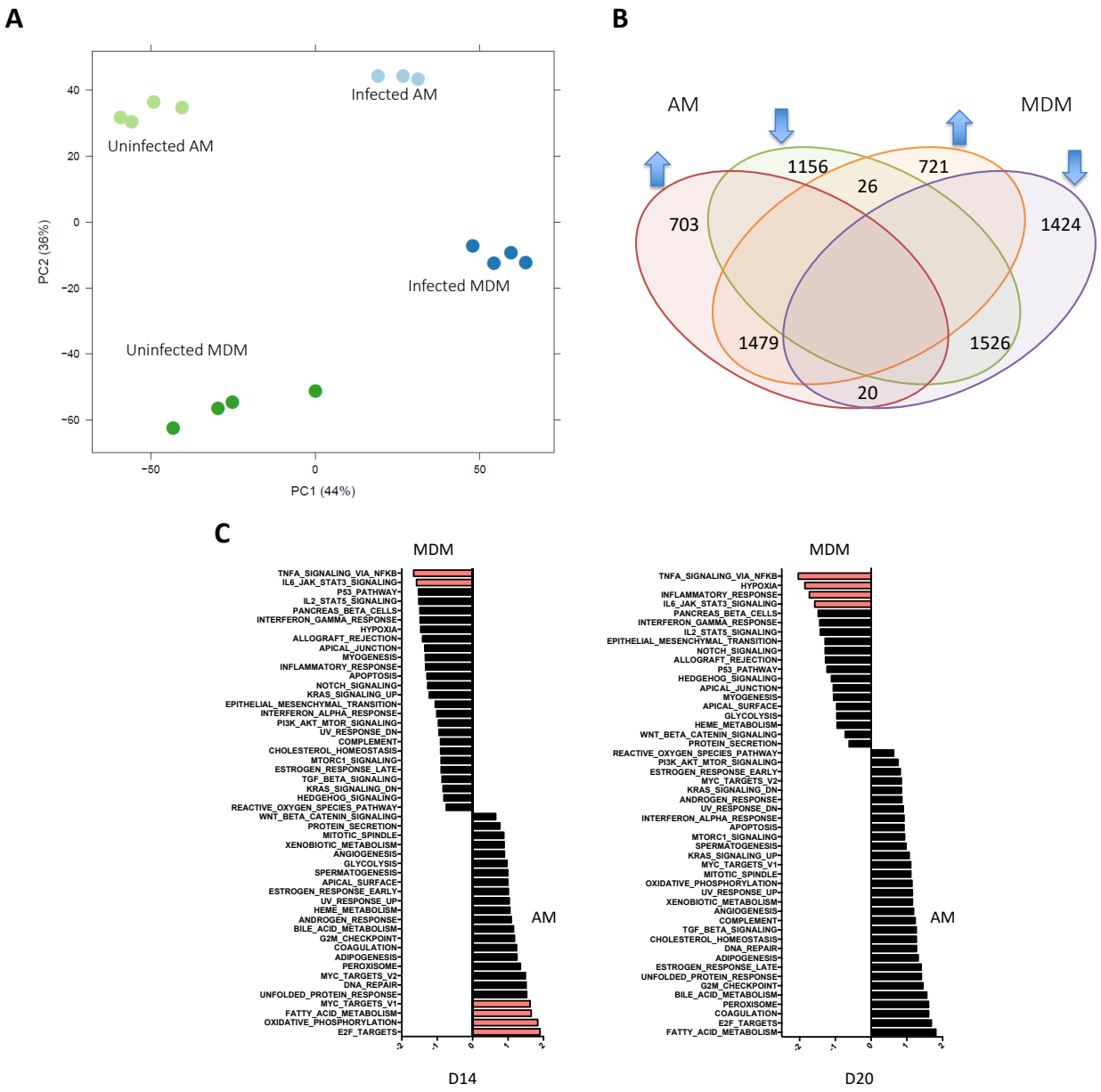

Figure 8: Transcriptional differences between AM and MDM at D20 and gene set enrichment analysis. Infected and uninfected AM and MDM were sorted from D20 mCherry infected animals for RNA-seq (each sample was generated from the lung cells sorted from 10 pooled mice, n=4 samples/group). (A) PCA plot showing the clustering of replicates within each group. (B) Venn diagram showing the number of differentially expressed genes (log2 foldchange>1, adjusted p-value<0.05) in infected AM and MDM (relative to uninfected cells of the same group). Arrows indicate up or downregulated genes. (C) Gene set enrichment analysis from D14 (Fig. 6) and D20. Preranked lists of gene expression in infected AM relative to infected MDM was used to test for enrichment of 50 hallmark gene sets. Red bars indicate FDR < 0.05.

pathways in infected MDM compared to infected AM. In addition, the hypoxia pathway was significantly enriched in MDM at D20. The pathways most enriched in infected AM included metabolic pathways such as oxidative phosphorylation and fatty acid metabolism. Given that AM are known to use fatty acid metabolism at steady state (43), this indicates that infection may not affect the metabolic programming of AM. In addition, multiple pathways related to proliferation were also enriched in infected AM.

Previous work has demonstrated that the metabolic state of Mtb-infected macrophages can impact their ability to restrict bacterial growth (46, 107). Specifically, glycolysis was shown to potentiate a proinflammatory, protective response. To validate the transcriptional metabolic differences, we stained lung cells with TMRM, a dye that is a readout of mitochondrial membrane potential. High membrane potential (more staining) can be indicative of cells using a mitochondria-based metabolic program such as oxidative phosphorylation. Lower membrane potential could be indicative of cell types using less mitochondrial metabolism, and potentially relying on glycolysis. We found that infected AM stained highly with TMRM at both D15 and D20 post infection, consistent with their transcriptionally predicted reliance on oxidative phosphorylation (Fig. 9A). Conversely, infected MDM shifted from being $TMRM^{hi}$ to $TMRM^{lo}$ between D15 and D20, suggesting that this cell type switches away from mitochondrial metabolism which correlates with the recruitment of CD4 T cells to the lung. Interestingly, when we bisect MDM at D20 by level of TMRM staining, we find that the $TMRM^{hi}$ cells are significantly more enriched in infected cells compared to the $TMRM^{lo}$ cells (Fig. 9B-C). Thus,

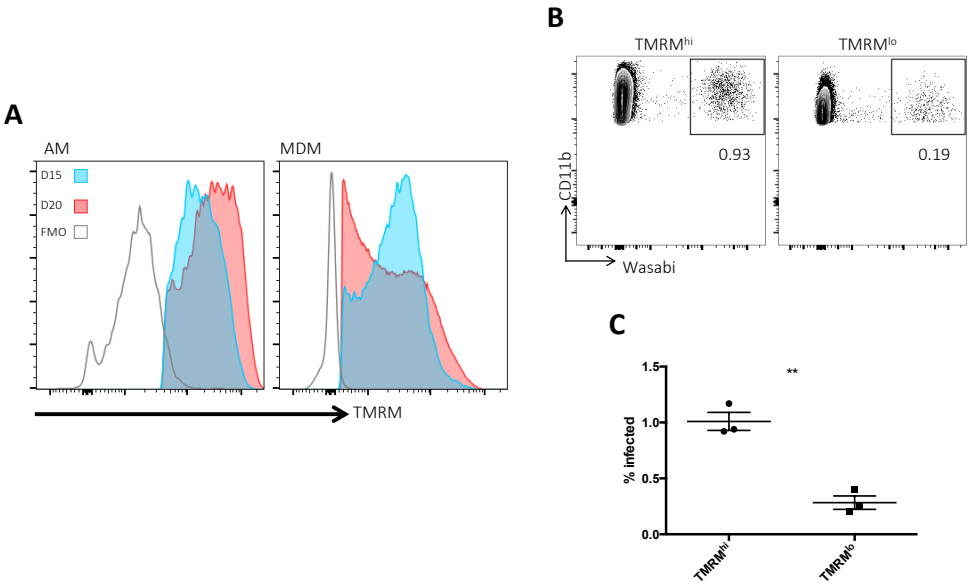

Figure 9: MDM shift away from mitochondrial metabolism during early infection.
Animals previously infected with Wasabi-Mtb were sacrificed at D15 and D20 and lung cell suspensions were incubated with the mitochondrial membrane dye TMRM prior to cell surface staining (n=3 mice/group). (A) Representative histograms showing the level of TMRM in AM and MDM at both time points. A fluorescence minus one (FMO) control is shown in gray. (B) Representative flow plots (gated on $TMRM^{lo}$ or $TMRM^{hi}$ MDM) showing the proportion of Wasabi+ cells at D20. (C) Proportion of $Wasabi^{+}$ $TMRM^{lo}$ or $TMRM^{hi}$ MDMs as determined by flow cytometry. Single-group comparisons were performed by unpaired t test. Data are presented as mean ± SEM. **$p < 0.01$. All experiments were performed at least 2–3 times.

this switch away from mitochondrial metabolism in the MDM seems to have a functional consequence upon either: the ability to clear infection, or the ability to prevent infection.

We next performed differential gene expression analysis to compare infected AM and MDM at D20. Through this, we identified MKP2, which was the 2nd most downregulated gene in infected AM compared to infected MDM. This gene, a MAP kinase regulatory enzyme, has previously been demonstrated to modulate the nitric oxide pathway in the context of other intracellular infections (108, 109). Thus, we next performed targeted analysis of the nitric oxide pathway itself (Fig. 10A). We found that genes involved in the import of the nitric oxide

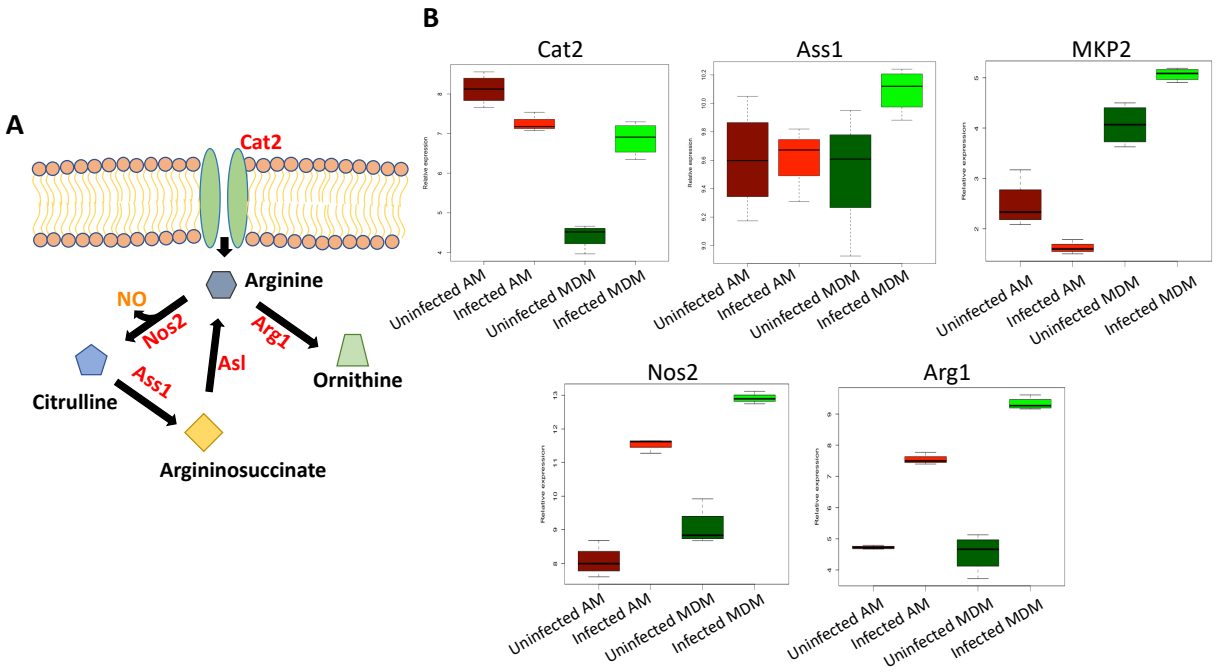

Figure 10: Differential expression of nitric oxide pathway-related genes at D20.
(A) Graphic showing genes important for the generation of nitric oxide (in red). Nitric oxide precursor and byproduct molecules are labeled in black. Adapted from Qualls et al., 2012. (B) Gene expression of the genes depicted in (A) at D20.

precursor arginine, as well as the recycling of arginine, were upregulated in infected MDM and downregulated in infected AM (Fig. 10B). Additionally, NOS2, the enzyme which catalyzes the formation of nitric oxide from arginine, was more highly expressed in infected MDM. To confirm that these transcriptional differences impact protein expression, we performed intracellular NOS2 staining (Fig. 11A-B). Here we observed that a higher proportion of infected MDM are $NOS2^{+}$ compared to infected AM. Coupled with previous reports that NOS2 is mycobactericidal (110), these data support the notion that nitric oxide production by certain infected macrophages may be important for protection. In line with this, when we assessed the lung bacterial burden in NOS2 KO chimeras, whereby WT or NOS2 KO bone marrow was transferred into irradiated hosts (WT>KO animals have WT hematopoietic cells and KO stromal cells, KO>WT animals have KO hematopoietic cells and WT stromal cells, WT>WT and

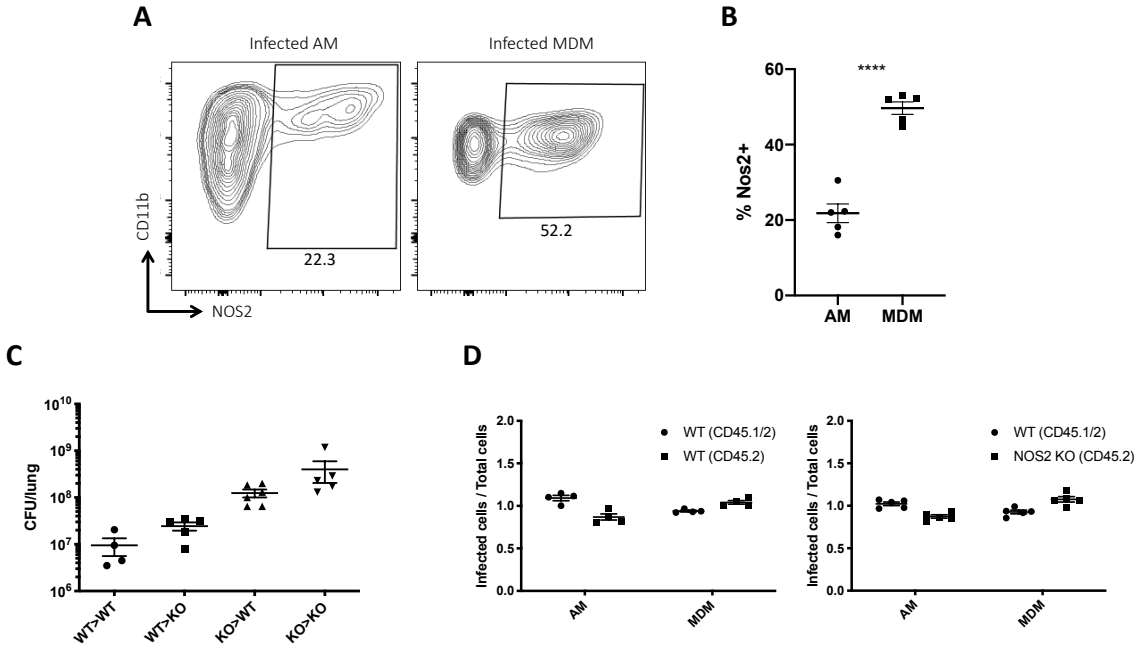

Figure 11: Differential NOS2 expression does not explain the superior protection of MDM.
(A) Representative flow plots showing NOS2 expression by infected AM and MDM at D20. (B) Proportion of infected AM and MDM which express NOS2 (n=5 mice/group) at D20. (C) Lung bacterial burden in NOS2 criss-cross chimeras at D30. (D) Normalized proportion of infected AM and MDM in mixed chimeras at D28. Chimeras containing either a 50:50 mix of WT (CD45.1/2): WT (CD45.2), or WT (CD45.1/2): NOS2 KO (CD45.2) were reconstituted in WT (CD45.1) hosts. Single-group comparisons were performed by unpaired t test and multiple-group comparisons by one-way ANOVA. Data are presented as mean ± SEM. ****$p < 0.0001$. All experiments were performed at least 2–3 times.

KO>KO are used as controls) we found that the major requirement for NOS2 was in hematopoietic cells, which is consistent with a previous report (52) (Fig. 11C). We next made WT:NOS2 KO mixed chimeras to test the hypothesis that the superior control of Mtb by MDM could be at least partially explained by their increased expression of NOS2. If this were true, we would have expected to observe an increase in the infection of infected KO MDM compared to WT MDM. Instead, we observed a similar proportion of infected WT and KO MDM as observed in WT:WT mixed chimeric controls (Fig. 11D). This is consistent with a recent report by Mishra et al., who have demonstrated that although NOS2 is important for Mtb control, unlike IFNγ, the requirement for NOS2 does not appear to be cell-intrinsic to the infected macrophage (52).

In order to identify whether there were other different transcriptional programs engaged by AM and MDM, we used a computational package called cMonkey2 (90). This analysis groups together genes which have similar expression patterns and also share transcription factor (TF) binding sites (Fig. 12A). Through this, 14 distinct biclusters were identified (Fig. 12B). In large part, the differential expression of these clusters correlated either with cell type (ex: bicluster 4, 6, 11) or infection state (ex: bicluster 1, 3, 5, 7, 8). Bicluster 9, however, appeared quite distinct as it was highly expressed only in infected MDM. Given that this cell type seems to be more protective, this bicluster had the potential to reveal a transcriptional signature of this protection. We next investigated the TFs predicted to regulate bicluster 9. The cMonkey2 analysis package uses 3 different TF motif discovery methods. 4 of the 23 TFs were identified using 2 out of these 3 methods (Table 2). The gene expression of 3 of these 4 transcription factors (not IRF2) directly or inversely mimicked the expression of the bicluster itself (Fig. 12C). Interestingly, these 3 TFs have all been previously been shown to play a regulatory role in proliferation (111-115). In line with this, our GSEA analysis also indicated that multiple pathways corresponding to proliferation were differentially expressed, specifically in the direction of infected AM being more proliferative than infected MDM (Fig. 12D). To validate this, we performed BrdU pulse experiments. Here, we observed that infected AM were indeed more proliferative than infected MDM (Fig. 13A-B). Interestingly, the infected AM also seemed to be proliferating more than uninfected AM, whereas at D22 MDM showed the opposite phenotype, infected cells exhibited less proliferation than uninfected cells. Thus, not only are AM more permissive to bacteria, but infection may somehow induce the expansion of this cell type and thus provide new targets for Mtb.

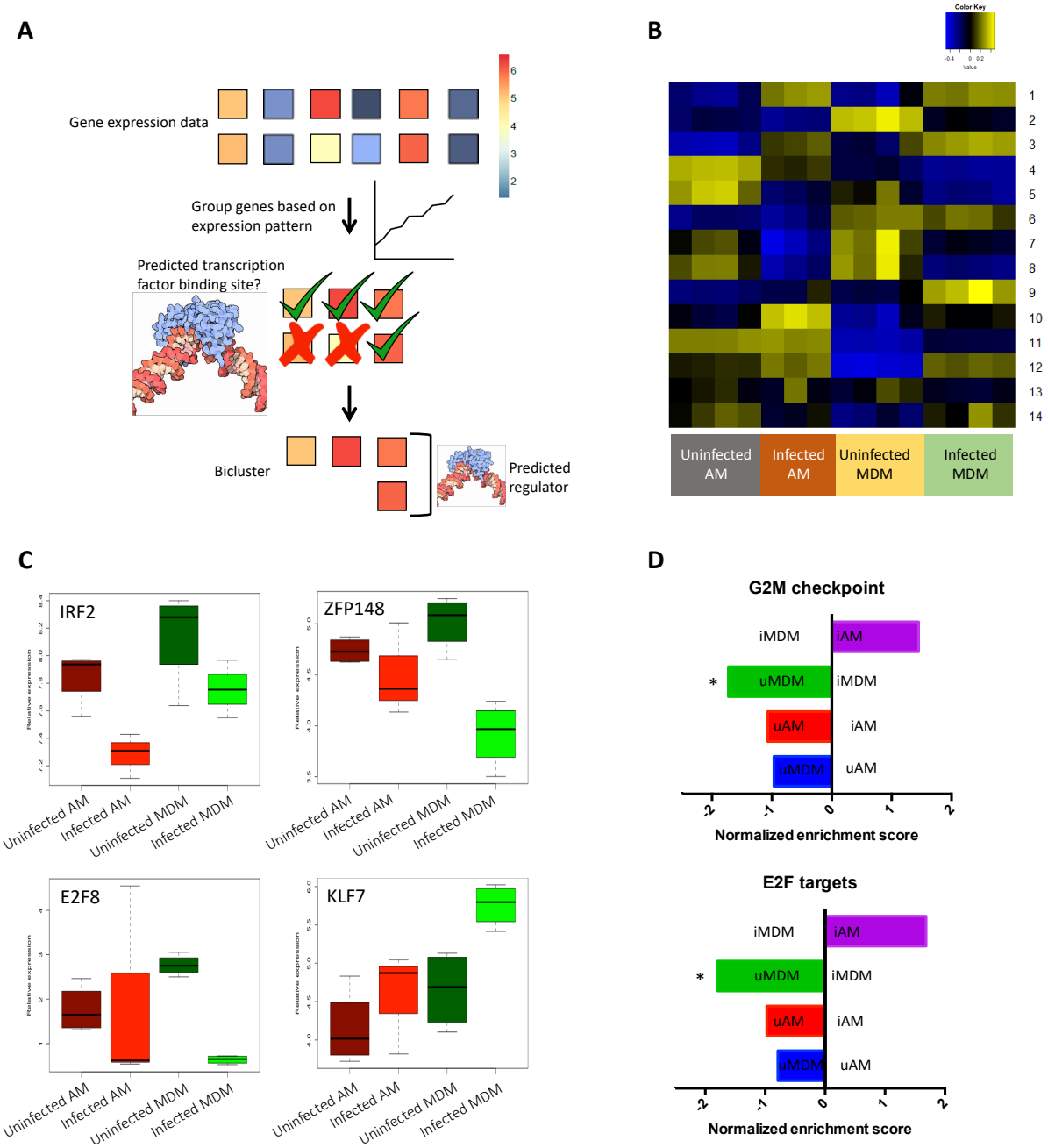

Figure 12: Transcription factor analysis of D20 infected macrophages predicts differential proliferation of infected macrophages.
(A) Schematic depicting the workflow, cMonkey2, used to identify transcription factor regulators of differentially expressed genes. First, gene expression data is clustered based on similar expression levels. Next, these clusters are iteratively refined based on whether genes share predicted transcription factor binding sites. This results in a series of biclusters which are unified based both on similar expression patterns as well as predicted transcription factors that regulate them. (B) Heatmap of the biclusters generated by cMonkey2 of infected and uninfected AM and MDM at D20. (C) Gene expression analysis of the 4 transcription factors identified with multiple algorithms (see Table 2) to regulate bicluster 9. (D) Gene set enrichment analysis of two pathways related to proliferation. Pairwise comparisons are shown between the different groups (u = uninfected, i = infected). The direction of the bars indicate which group was enriched in the gene set. * indicates FDR < 0.05.

MEME	TFBS_DB	WEEDER
ARID3A	DBP	E2F6
E2F8	GRHL1	E2F8
EBF1	MAFB	ELK3
FOXA3	MECOM	FOSL1
FOXD1	MESP1	GLIS3
FOXJ2	MXD3	GRHL2
GLIS3	NR4A3	IRF2
IRF2	RXRA	KLF7
KLF7	SOX17	SOX6
ZFP148	SPIC	TAL2
ZFP410	TCF7L2	ZBTB14
ZFP516	TRP73	ZFP148
ZIC1	XBP1	

Table 2: Predicted regulators of bicluster 9
The cMonkey2 package uses 3 different algorithms to predict transcript factor binding sites (MEME, TFBS_DB, and WEEDER). This table depicts the transcription factors which were predicted by each of the algorithms to regulate bicluster 9.

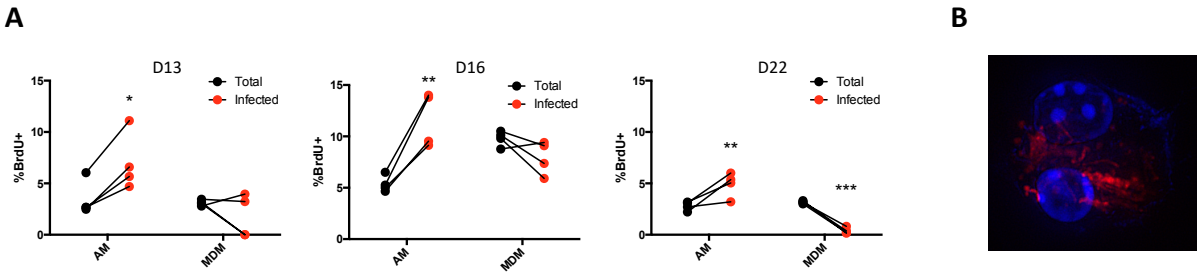

Figure 13: Infected macrophages display differential proliferation
(A) Proportion of AM and MDM which have taken up BrdU at the given timepoints (n=3-4 mice/group/timepoint). (B) Fluorescence image of an infected AM at D14 which seems to be in the process of dividing. Single-group comparisons were performed by paired t test. *$p < 0.05$,** $p < 0.01$, ***$p < 0.001$. All experiments were performed at least 2–3 times.

Finally, given these differences in the responses of AM and MDM during Mtb infection, we sought to characterize how the bacteria itself was responding to these distinct host niches. To achieve this, we took advantage of a recently described method for enrichment of Mtb RNA from within mammalian macrophages which can then be used to perform RNA-seq (91). We sorted AM and MDM from D20 infected animals and sequenced the transcriptomes of Mtb from each of these cell types. When we perform PCA, we observe that the Mtb recovered from AM cluster distinctly from the Mtb recovered from MDM (Fig. 14A). We next investigated the

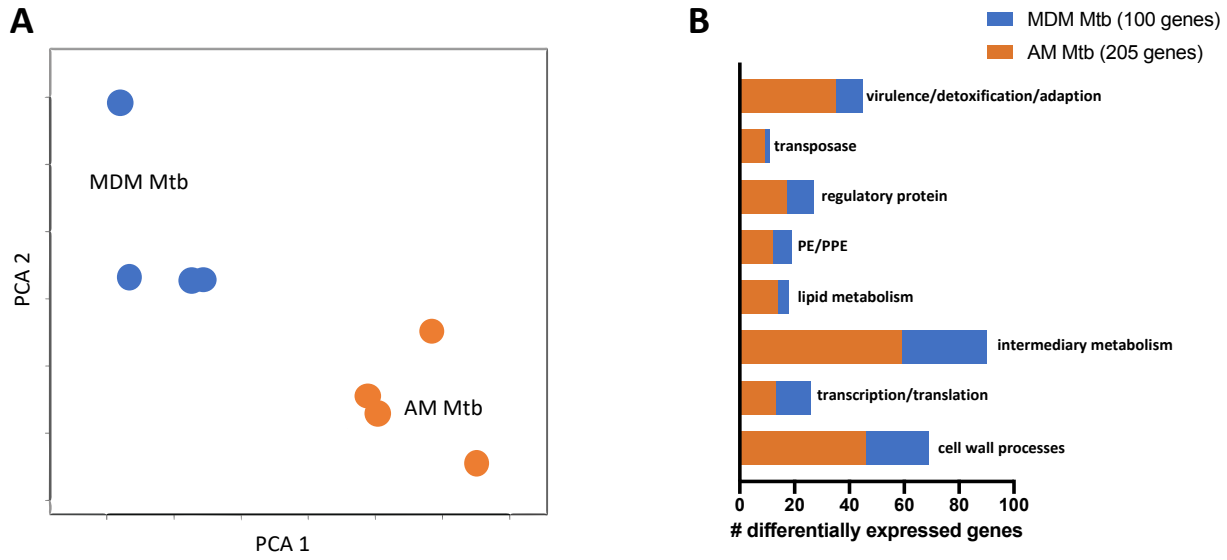

Figure 14: Mtb segregate transcriptionally on the basis of cell type.
(A) PCA plot of RNA-seq data from Mtb sorted from infected AM and MDM at D20 (each sample was generated from the lung cells sorted from 2 pooled mice, n=4 samples/group). (B) Classification of the types of genes which were significantly differentially expressed in the Mtb recovered from each cell type.

functional processes the differentially expressed genes were associated with (Fig. 14B). There were more than twice as many differentially expressed genes in AM Mtb compared to MDM Mtb. However, the major processes these genes were involved in for both cell type was intermediary metabolism and cell wall processes. Within this set of differentially expressed genes were transcripts involved in the type VII secretion system of Mtb. This system provides

the means for transporting proteins out of the bacterial cell. The Mtb genome encodes five of these secretion systems: ESX1-ESX5 (116). ESX-1, -3, and -5 have previously established roles in virulence, while the function of ESX-2 and ESX-4 is less clear. Interestingly, all of the differentially expressed genes associated with ESX-1 and ESX-5 were more highly expressed in the AM Mtb, while the sole ESX-4 gene was higher in MDM Mtb (Fig. 15). Thus, the AM Mtb seem to be better engaging known virulence genes in the cell type in which they are growing better.

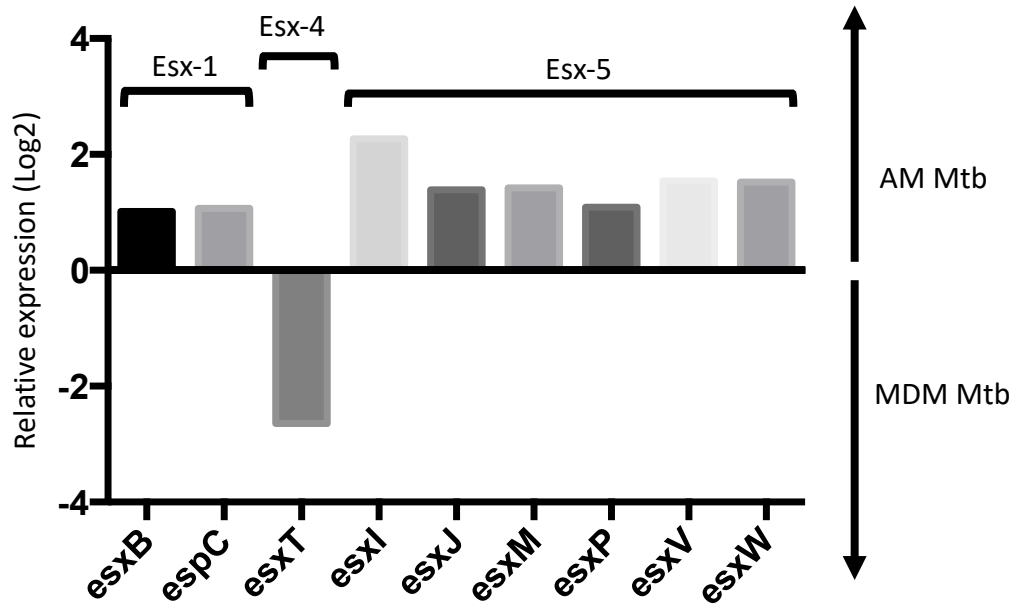

Figure 15: Mtb secretion system genes are differentially expressed in infected macrophages.
Relative expression of genes related to the ESX secretion systems in AM and MDM. Brackets indicate specific secretion system each gene is associated with.

Lastly, we attempted to understand whether the transcriptional state of the bacteria aligned with any known stress responses. One of the stresses that Mtb encounters within the host is oxygen deprivation or hypoxia (117). During TB disease, the aggregation of immune cells at the site of infection leads to the formation of a structure called the granuloma. The purpose of the granuloma is to wall off the bacteria, preventing its spread, and oxygen levels are often low at

the center of this structure. While this hypoxic environment can aid in bacterial killing (118), Mtb can also sense and respond to this change by engaging transcriptional programs that permit survival through alterations in metabolism and energy use (119, 120). Our collaborators have previously performed a detailed time course of the transcriptional response of Mtb grown in liquid culture to hypoxia. Here, oxygen levels are gradually reduced over 40 hours and maintained at 0% for around 70 hours (Fig. 16A). By sampling the bacteria throughout this process, they have identified transcriptional signatures that distinguish: normoxia, oxygen depletion, early hypoxia, mid hypoxia, late hypoxia, and resuscitation (oxygen reintroduction) (Fig. 16B-C). We used these signatures to test whether differentially expressed Mtb genes from AM or MDM aligned with a particular phase of hypoxia (Table 3). Here, we found that there was highly significant overlap between genes upregulated in MDM bacteria and those that define late hypoxia. In contrast, the genes upregulated in AM bacteria were most significantly associated with mid hypoxia, though there was also significant association with early hypoxia and resuscitation. These results support the idea that MDM, the more protective cell type, presents a more hostile environment for Mtb, as is evidenced by the late hypoxia signature identified.

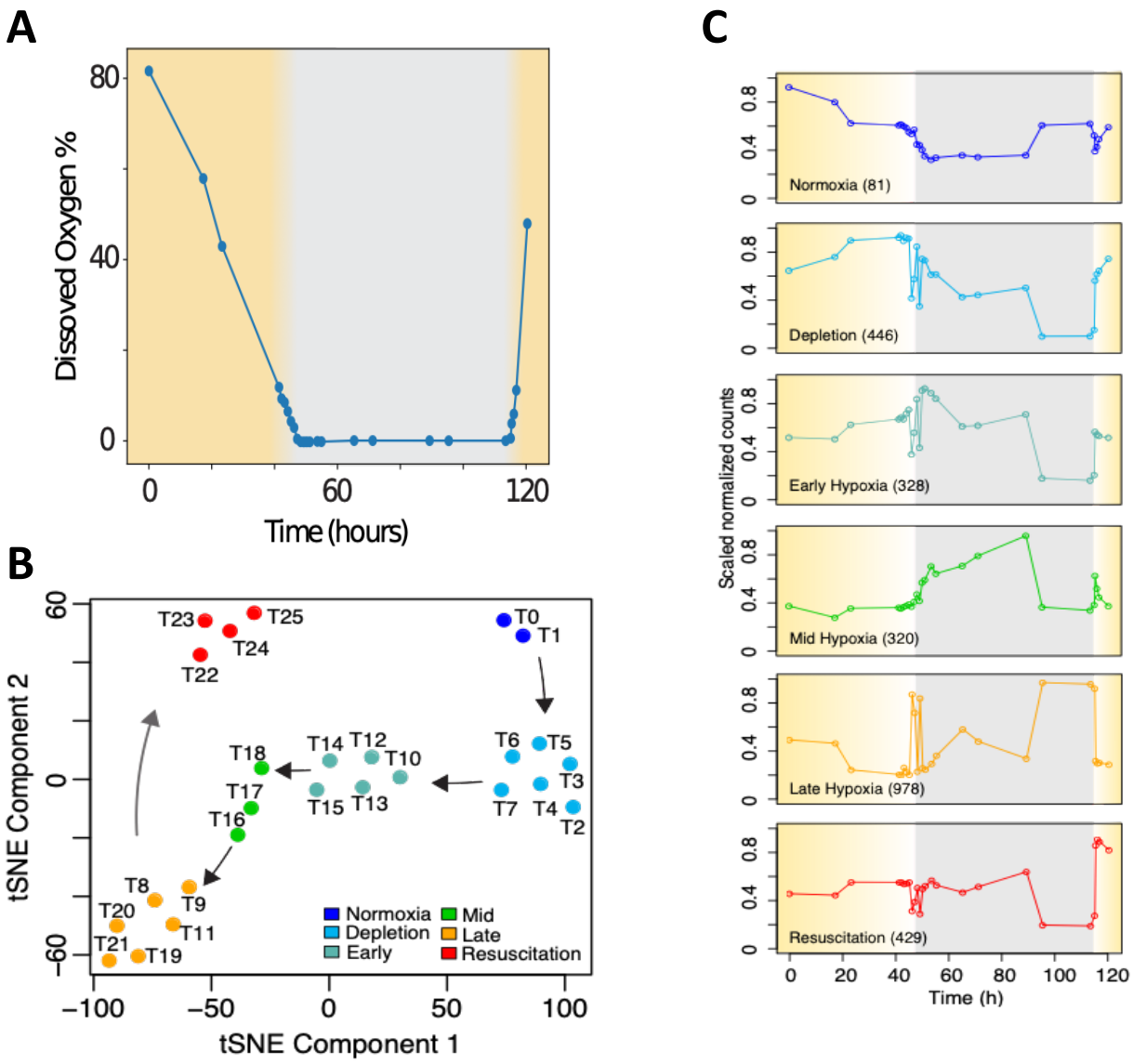

Figure 16: Characterization of transcriptional hypoxia states in Mtb.
(A) Mtb was grown in liquid culture and oxygen was gradually depleted from time 0 to 40hrs. Hypoxia was maintained until 120hrs before reaeration. Dots indicate timepoints when samples were taken for RNA-seq. (B) PCA plot showing the clustering of RNA-seq data from each timepoint sampled. (C) Genes were clustered based on the phase when they were most highly expressed. Normalized counts for the genes in each set are overlaid on the time course.

Cell type	# enriched genes	hypoxia state	# hypoxia state genes	# intersect genes	adj p value
MDM Mtb	179	early_hypoxia	327	6	0.99338
MDM Mtb	179	mid_hypoxia	320	5	0.9971
MDM Mtb	179	late_hypoxia	978	69	6.3E-06
MDM Mtb	179	resuscitation	429	5	0.99995
AM Mtb	317	early_hypoxia	327	35	0.02392
AM Mtb	317	mid_hypoxia	320	41	0.00056
AM Mtb	317	late_hypoxia	978	49	0.99997
AM Mtb	317	resuscitation	429	49	0.00256

Table 3: Mtb in AM display a transcriptional signature of late hypoxia.
Differentially expressed genes enriched in bacteria recovered from AM and MDM were tested for overlap with hypoxia state gene sets (defined in Fig. 15C).

Discussion

The route of Mtb infection, phagocytosis, permits many different types of immune cells to potentially become infected. However, the cell-type specific responses of the major phagocyte targets of *in vivo* infection remain understudied. In addition, while many new vaccine candidates aim to boost the CD4 T cell response, the capacity of this cell type to confer early immunity is unknown. Here, we found that Mtb-specific CD4 T cells are unable to provide protection during the first week of infection. T cells do provide protection at two weeks post-infection, once MDM become the major infected cell type. Through a comparative analysis of AM and MDM, we observe that MDM are more protective and better engage antibacterial programs than AM. Our host transcriptional analysis also predicted there would be differences in metabolism and proliferation between the two cell types, which we validated experimentally. Finally, we also performed Mtb transcriptional analysis and found that bacteria recovered from MDM seemed to be experiencing sustained hypoxia compared to bacteria in AM.

These results are consistent with a number of recent studies which have also characterized early phagocyte responses during Mtb infection (46, 53). Huang et al. found that recruited macrophages were more restrictive to Mtb while AM were more permissive using a number of bacterial fitness reporter strains. They also performed transcriptional analyses which aligns with our data with regard to differences in: replication, metabolism, and proinflammatory signaling. Rothchild et al. performed a detailed time course of the transcriptional response of infected AM starting 1d post-infection. Here, they saw that the transcriptional changes that occur upon AM infection are remarkably non-inflammatory. Together, these studies provide strong evidence that the natural response of the AM may be detrimental to the host and could contribute to establishing a state of infection which is difficult to clear. The studies performed in this chapter extend on these publications by considering how the phenotype of the AM may negatively affect the ability of the adaptive immune response (i.e. CD4 T cells) to respond productively and rapidly. In addition, we have begun to characterize the response of the bacteria within these macrophages, which likely influences host immunity and could reveal new avenues for therapeutic intervention.

A number of open questions related to this work remain. Given the permissive, non-inflammatory nature of the AM, is it possible to make this cell type more bactericidal? From these studies, we do not find an obvious defect in the AM with regard to its ability to present antigen or respond to IFNγ. The positioning of this cell type in the lung airways necessitates strong regulatory mechanisms be in place in order to prevent excessive activation which could lead to organ damage. Perhaps modulation of one or more of the inhibitory receptors known to be expressed on the surface of AM could release the brakes and permit better bacterial control. While this work focused on early Mtb infection, future studies should investigate the dynamics

of phagocyte immunity during chronic infection. For example, what is the proportion of different cell types infected at late time points? Previous work has demonstrated that chronic infection leads to CD4 T cell exhaustion, but what about the functionality of the phagocytes? These studies could help to inform new strategies for post-exposure prophylaxis or therapeutics.

CHAPTER 4: BCG-induced T cells shape Mycobacterium tuberculosis infection before reducing the bacterial burden

Introduction

Bacillus Calmette-Guerin (BCG), the current tuberculosis (TB) vaccine, is effective at preventing disseminated disease in infants and young children (121). However, in most settings it provides little or no protection against adult pulmonary TB, the transmissible form of disease (19). Thus, despite widespread BCG immunization for nearly a century, Mycobacterium tuberculosis (Mtb) kills over 1.5 million people every year, more than any other single infectious agent (2). A better TB vaccine is urgently needed, but attaining this goal has been surprisingly difficult (95). Furthermore, because BCG reduces childhood mortality, a new vaccine will likely be added to a regimen that includes BCG, rather than replace it (26). To develop a strategy that builds upon BCG-mediated protection, we must first understand how BCG shapes immunity to Mtb, especially during early stages of infection when protective immunity is established.
In mice, pulmonary Mtb burdens are equivalent between BCG-immunized and control mice until two weeks after infection (122). The failure of BCG to impact the Mtb burden during the first two weeks of infection has been attributed to the delayed arrival of T cells in the lung (123). However, BCG-specific T cells have been shown to be present in the lungs (124) of immunized mice even prior to Mtb challenge, indicating that impaired T cell recruitment cannot fully account for the inability of BCG to induce early protection.

In this study, we utilized the mouse model to investigate the impact of BCG on the early immune response to Mtb infection. Our findings reveal unexpected roles for CD4 T cells in: 1) accelerating the translocation of Mtb-infected alveolar macrophages (AM) into the lung interstitium; 2) recruiting monocyte-derived macrophages; and 3) promoting the early transfer of Mtb from AM to other phagocytes. Despite these effects, a vaccine-induced reduction in the lung

bacterial burden does not occur until co-localization of CD4 T cells with infected macrophages, which is delayed until two weeks post-infection even in vaccinated animals.

Results and Discussion

BCG vaccination promotes Mtb egress from AM early in infection.

To understand the effects of BCG immunization on early Mtb infection, we examined the pulmonary Mtb burdens in BCG-immunized and control mice. Consistent with prior reports (122, 123), lung burdens rose similarly in both groups through two weeks (Fig. 1A). At D15, the Mtb burden in the immunized group began to diverge and was reduced by one log by D21. These findings are consistent with the idea that BCG-induced immunity is not initiated until the third week of Mtb infection.

We recently found that Mtb first infects AM before disseminating to other cells, including neutrophils (PMN) and monocyte-derived macrophages (MDM) (45). As tissue-resident and recruited phagocytes have been shown to differ in their capacity to curb Mtb replication (46, 58), we next asked whether immunization alters the proportions of cell types that harbor infection. Consistent with the similar Mtb burdens at D14, the numbers of cells harboring fluorescent Mtb (Mtb-mCherry) were also similar in each group (Fig. 1B). Surprisingly, even at this early phase, we observed a dramatic shift in the composition of infected cells. At D14, by gating on $mCherry^+$ cells, we found that the proportion of Mtb-infected AM was significantly reduced in immunized animals compared to controls, with a corresponding increase in infected PMN and MDM (Fig. 1C-D). There was no effect on the infection of DCs (Supplemental Fig. 1A). We confirmed these findings using confocal microscopy and quantitative histocytometry (88), wherein most Mtb was within $SiglecF^+$ AM at D14 in controls but within $CD11b^+$ $SiglecF^-$

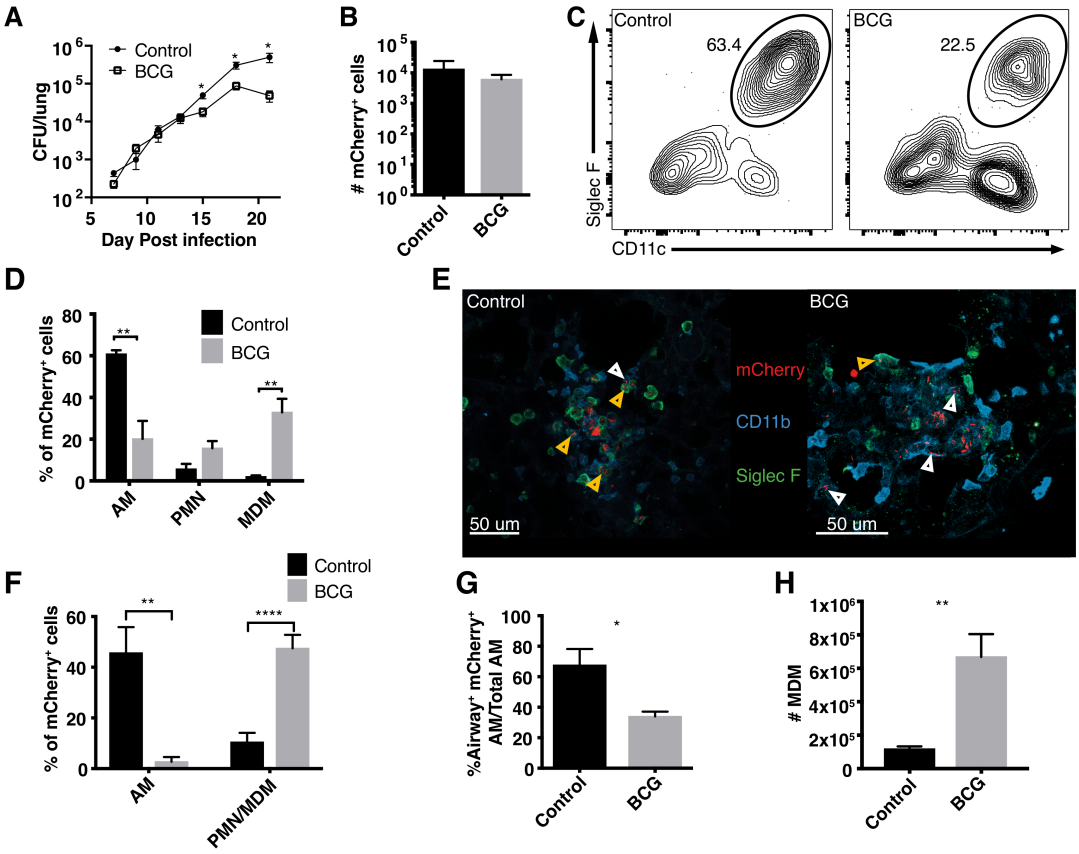

Figure 1: BCG vaccination promotes Mtb egress from AM early in infection.
(A) Mtb burden in the lungs of mice that did or did not receive BCG (n=4 mice/group/ timepoint). (B) Total number of mCherry$^+$ lung cells at D14 by flow cytometry (n=4-5 mice/group). (C) Representative flow plot of the proportion of mCherry$^+$ cells identified as CD11c$^+$ Siglec-F$^+$AMs at D14. (D) Composition of mCherry$^+$ lung cells (AM: CD11c$^+$ Siglec-F$^+$, PMN: CD11b$^+$ Ly6G$^+$, MDM: CD11b$^+$ CD64$^+$) at D14 by flow cytometry (n=4-5 mice/group). (E) Representative images of the lung at D14 showing infected Siglec F$^+$ AM (orange arrows) and infected Siglec F$^-$ CD11b$^+$ cells (white arrows). (F) Composition of mCherry$^+$ lung cells at D14 by quantitative histocytometry (n=6-8 infectious foci from 2 mice/group). (G) Ratio of airway label positive infected AM at D14 (n=5 mice/group). (H) Number of MDM in the lung at D14 by flow cytometry (n=4-5 mice/group). Single-group comparisons were performed by unpaired t test. Data are presented as mean ± SEM. *p < 0.05, **p < 0.01, ****p < 0.0001. All experiments were performed at least 2–3 times.

cells (primarily PMN and MDM) in immunized mice (Fig. 1E-F). As Mtb dissemination to PMN and MDM requires translocation of infected AM to the lung interstitium (45), we next assessed whether this translocation was accelerated in immunized mice. Indeed, intratracheal antibody administration, which specifically labels alveolar-localized cells (45), revealed significantly increased interstitial localization (label-negative) of infected AM in immunized mice at D14 (Fig. 1G). Importantly, the changes in infected cell types was independent of changes in AM or

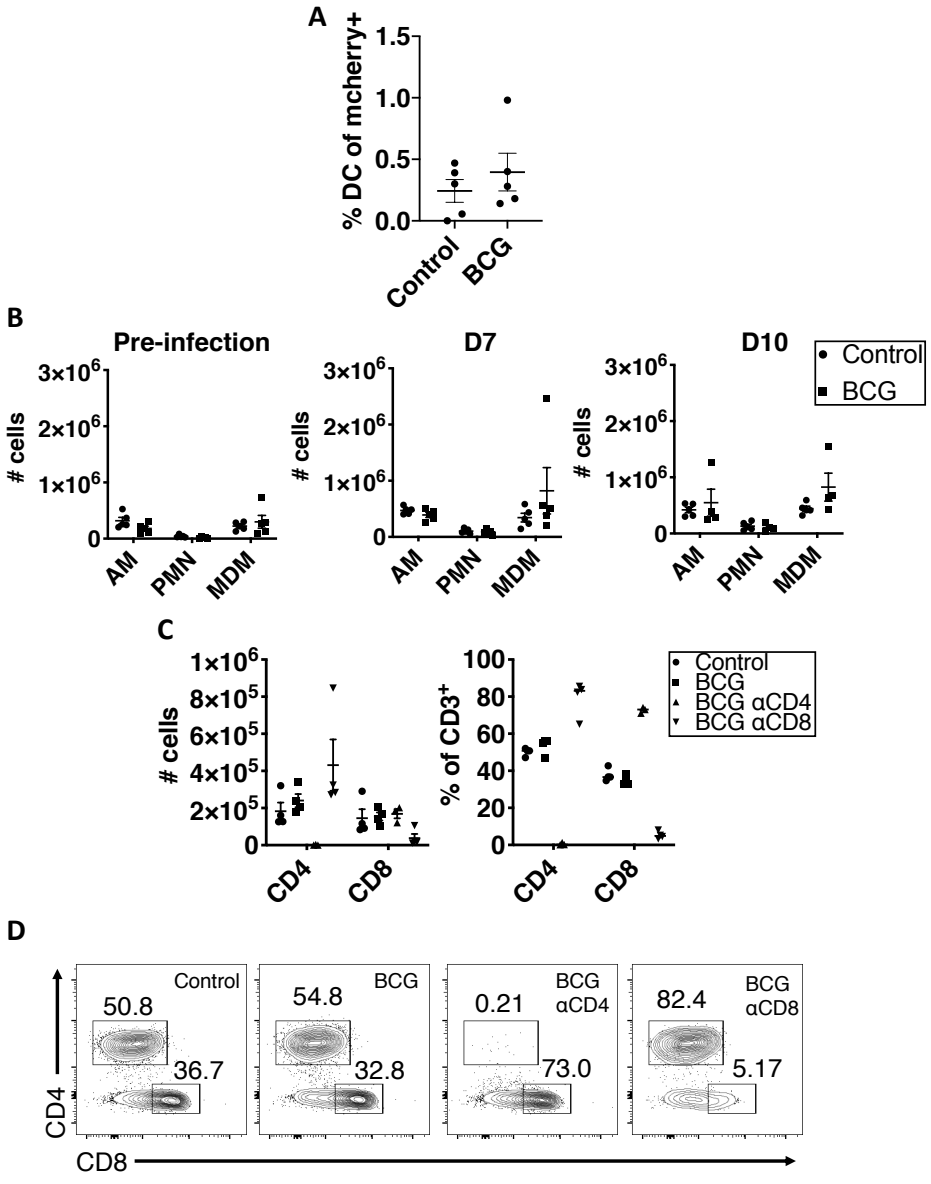

Supplemental Figure 1: Quantification of infected DCs, early phagocyte cellularity, and T cell depletion efficacy. (A) Proportion of mCherry+ cells which were identified as DCs (CD11c+ MHCII+ CD64-) at D14 post-infection. (B) Quantification of the number of AM, PMN, and MDM in the lungs of animals prior to and following Mtb infection as determined by flow cytometry (n=4-5 mice/group). Single-group comparisons were performed by unpaired t test. Data are presented as mean ± SEM. (C) Total numbers and proportions of CD3+ CD4 and CD8 T cells in the lungs of control, BCG, and BCG animals that were treated with CD4 or CD8-depleting antibodies (n=4 mice/group). (D) Representative flow plots showing the proportion of CD3+ cells that are CD4 and CD8 T cells recovered from the lungs.

PMN cellularity as we found no differences in the numbers of these cells following immunization or infection (Supplemental Fig. 1B). Finally, immunization significantly enhanced

MDM recruitment to the lung at D14 (Fig. 1H), which was not observed at earlier time points or prior to infection (Supplemental Fig. 1B), suggesting that the accelerated recruitment of MDM in immunized mice begins between D10 and D14. Thus, although BCG does not impact the pulmonary Mtb burden in the first 2 weeks of infection, it accelerates the translocation of infected AM from alveoli to the lung interstitium, MDM recruitment, and Mtb dissemination to PMN and MDM.

BCG accelerates the recruitment of antigen-specific T cells to the lung following Mtb infection.

This unexpected impact of BCG on the early dynamics of infection led us to next investigate how immunization affects the kinetics of T cell recruitment to the lung. Before infection, antigen-specific CD4 (Ag85B) and CD8 (TB10.4) T cells could be identified in lung cell suspensions of immunized mice (Fig. 2A-C). Although ~25% of the Ag85B-specific CD4 T cells were located in the lung parenchyma (as evidenced by their failure to stain with i.v. CD45 antibody), virtually all of the TB10.4-specific CD8 T cells resided in the vasculature (Fig. 2D). This difference is consistent with a recent report that lung CD4 T resident memory cells may be maintained for longer than CD8 T cells (125). Following infection, immunized mice had significantly more TB10.4-specific cells, as well as Ag85B-specific CD4 T cells, in the lung parenchyma than controls as early as D10; by D14 they contained >5-fold more (Fig. 2B-C). Thus, BCG induces a small population of lung-resident Mtb-specific CD4 T cells prior to infection. After infection, BCG accelerates the pulmonary accumulation of both CD4 and CD8 Mtb-specific T cells, even before impacting the Mtb burden.

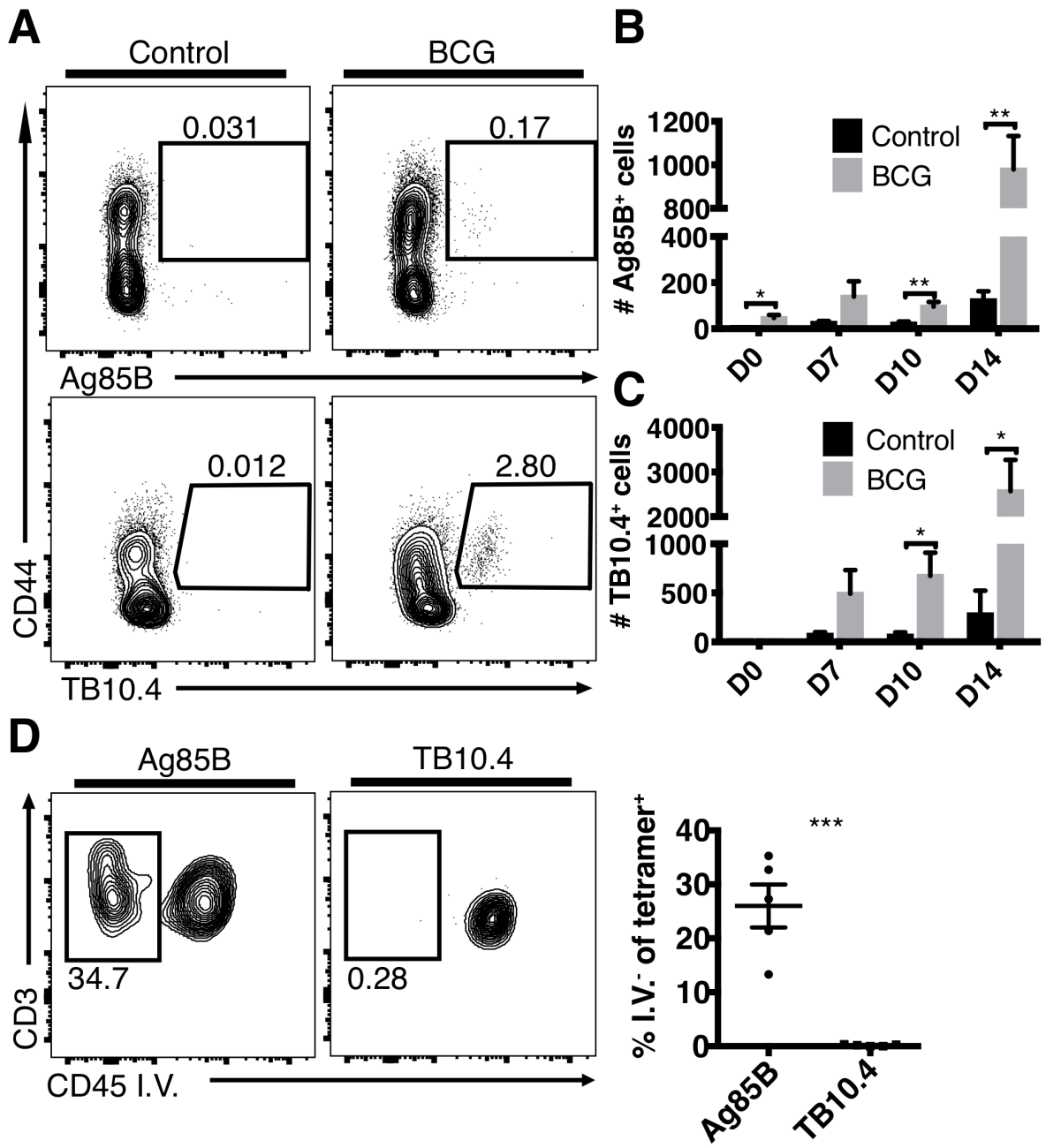

Figure 2: BCG accelerates the recruitment of antigen-specific T cells to the lung following Mtb infection. Time course of the number of tetramer-specific T cells in the lung. Mice received i.v. CD45 antibody prior to sacrifice. (A) Representative flow plots showing Ag85B-specific ($CD3^+CD4^+$) and TB10.4-specific ($CD3^+CD8^+$) T cells in the lungs of control and immunized mice prior to infection. The $tetramer^+$ cells in immunized mice are further gated on CD45 $i.v.^-$ to determine the proportion in the lung parenchyma. Total number of $i.v.^-$ Ag85B-specific (B) and TB10.4-specific (C) cells in the lungs of control and immunized mice (n=3-5 mice/group/timepoint). (D) Proportion of $tetramer^+$ cells that are $i.v.^-$ in immunized mice at D0 (n=5 mice/group). Single-group comparisons were performed by unpaired t test. Data are presented as mean ± SEM. *$p < 0.05$, **$p < 0.01$, ***$p < 0.001$. All experiments were performed at least twice.

CD4 T cells are required for the accelerated transfer of Mtb from AM to recruited phagocytes.

Given the presence of lung-resident Mtb-specific T cells in immunized mice prior to infection, we next determined whether T cells play a role in the accelerated transfer of Mtb from AM to other myeloid cells. CD4 or CD8 T cells were depleted from immunized mice beginning 1 day prior to Mtb-mCherry infection and lung cells were assessed at D14 (Supplemental Fig. 1C-D). In the absence of CD4 T cells, the accelerated transfer of Mtb from AM to PMN and MDM was partially reversed, whereas CD8 T cell depletion had no effect (Fig. 3A). Interestingly, the accelerated MDM recruitment (Fig. 1H) was also abolished by CD4 depletion (Fig. 3B). To assess whether antigenic recognition by CD4 T cells, even in the absence of vaccination, was sufficient to transfer Mtb infection from AM to other phagocytes, we adoptively transferred transgenic Mtb ESAT-6-specific CD4 T cells (C7), or OVA-specific CD4 T cells (OT-II) as a control, into unimmunized mice that were infected with Mtb 10 days prior. Four days later (D14) we observed that ESAT-6-specific, but not OVA-specific T cells, were sufficient to induce the transfer of infection out of AM (Fig. 3C), suggesting that antigen-specific CD4 T cell activation is needed to mediate this effect. Finally, we investigated whether direct recognition of Mtb-infected cells by CD4 T cells was required for the early dissemination out of the AM niche. WT (CD45.1):MHCII$^{-/-}$ (CD45.2) mixed bone marrow chimeras were generated, BCG immunized, and infected with Mtb-mCherry to test whether MHCII$^{-/-}$ AM, which cannot present antigen to CD4 T cells, would retain Mtb longer than WT AM. At D14, BCG induced the accelerated transfer of Mtb from AM to other myeloid cells irrespective of intrinsic MHCII expression (Fig. 3D). Taken together, BCG-induced CD4 T cells promote the early transfer of Mtb from AM to other myeloid cells in a process that seems to require antigenic recognition, but

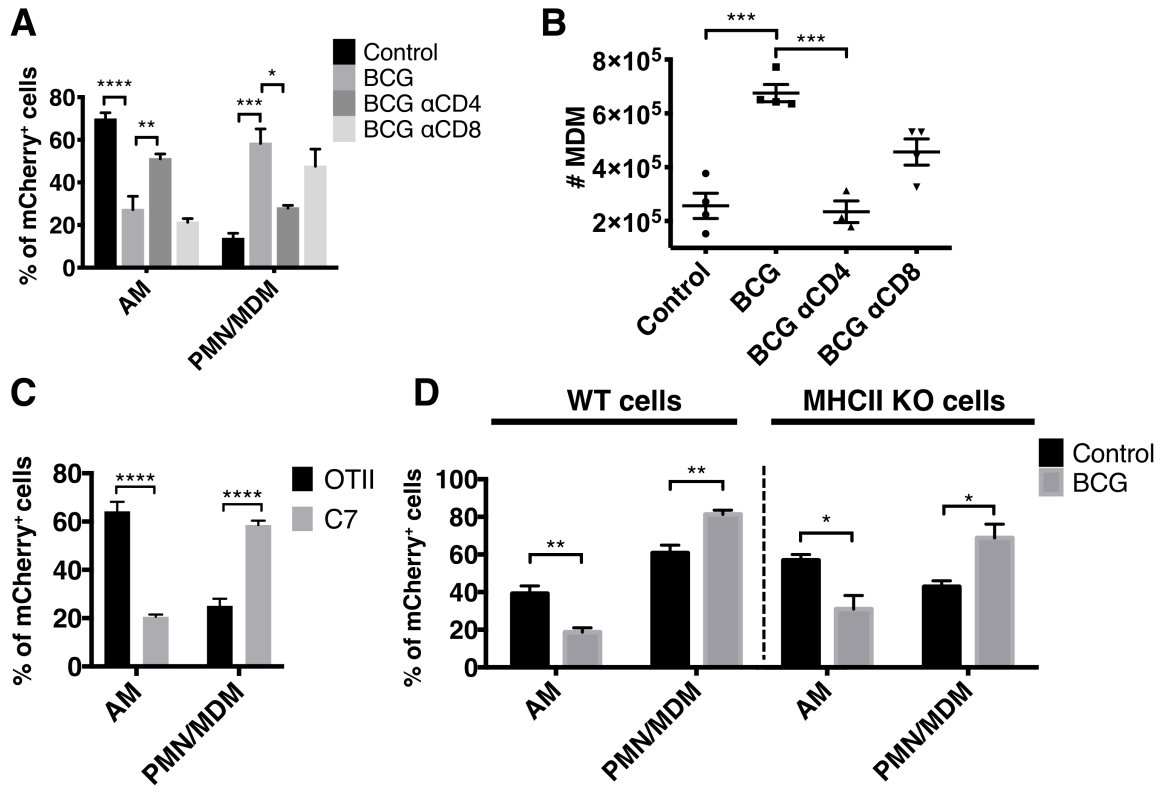

Figure 3: CD4 T cells are required for the accelerated transfer of Mtb from AM to recruited phagocytes. (A) Composition of mCherry$^+$ cells in control, immunized, and T cell-depleted immunized mice at D14 (n=4 mice/group). (B) Total number of MDM as in (A). (C) Composition of mCherry$^+$ cells at D14 in mice that received either OTII or C7 Th1 cells at D10 (n=5 mice/group). (D) Composition of CD45.1$^+$ WT (left) and CD45.2$^+$ KO (right) mCherry$^+$ cells in control and immunized mixed bone marrow chimeras at D14 (n=3-4 mice/group). Single-group comparisons were performed by unpaired t test (C-D) and multiple-group comparisons by one-way ANOVA (A-B). Data are presented as mean ± SEM. *$p < 0.05$, **$p < 0.01$, ***$p < 0.001$, ****$p < 0.0001$. All experiments were performed at least twice.

does not require direct cognate interactions between T cells and Mtb-infected AM. Our finding that CD4 T cells promote MDM recruitment to the lung, thereby providing new bacterial targets, may help explain the increased proportion of infected MDM in immunized animals. This recruitment likely relates to T cell production of cytokines, such as IFN-γ and TNF, which are known to trigger the release of chemokines that act on MDM, i.e., CCL2 and CXCL10 (126).

BCG-induced CD4 T cells are initially activated distal to the site of Mtb infection.

Given that CD4 T cells seem to induce the transfer of infection independent of direct interactions with infected cells, we next sought to monitor T cell activation in the lung using phospho-S6 (pS6), a ribosomal protein that is rapidly phosphorylated after TCR engagement and can be detected both by flow cytometry and confocal microscopy. Although previous work has shown that pS6 specifically marks T cells that have recently engaged their TCR (peaking at 4h and resolving within 24h) under homeostatic conditions (127), we first confirmed this specificity in the context of Mtb-infected lungs by showing robust pS6 expression by adoptively transferred TCR transgenic Mtb-specific (ESAT-6; C7) CD4 T cells compared to irrelevant TCR transgenic T cells (OVA-specific) (Supplemental Fig. 2A). Next, we examined pS6 in the endogenous, polyclonal CD4 T cell population to monitor the kinetics and location of TCR signaling during early Mtb infection. While there were very few $pS6^+$ CD4 T cells in the lungs of either control or immunized mice prior to Mtb challenge, as measured by flow cytometry (Supplemental Fig. 2B), $pS6^+$ CD4 T cells were readily identified in the vasculature of both unimmunized and immunized mice by D10, and were present in higher numbers in the lung parenchyma of immunized mice compared to controls (Supplemental Fig. 2C, Fig. 4A).

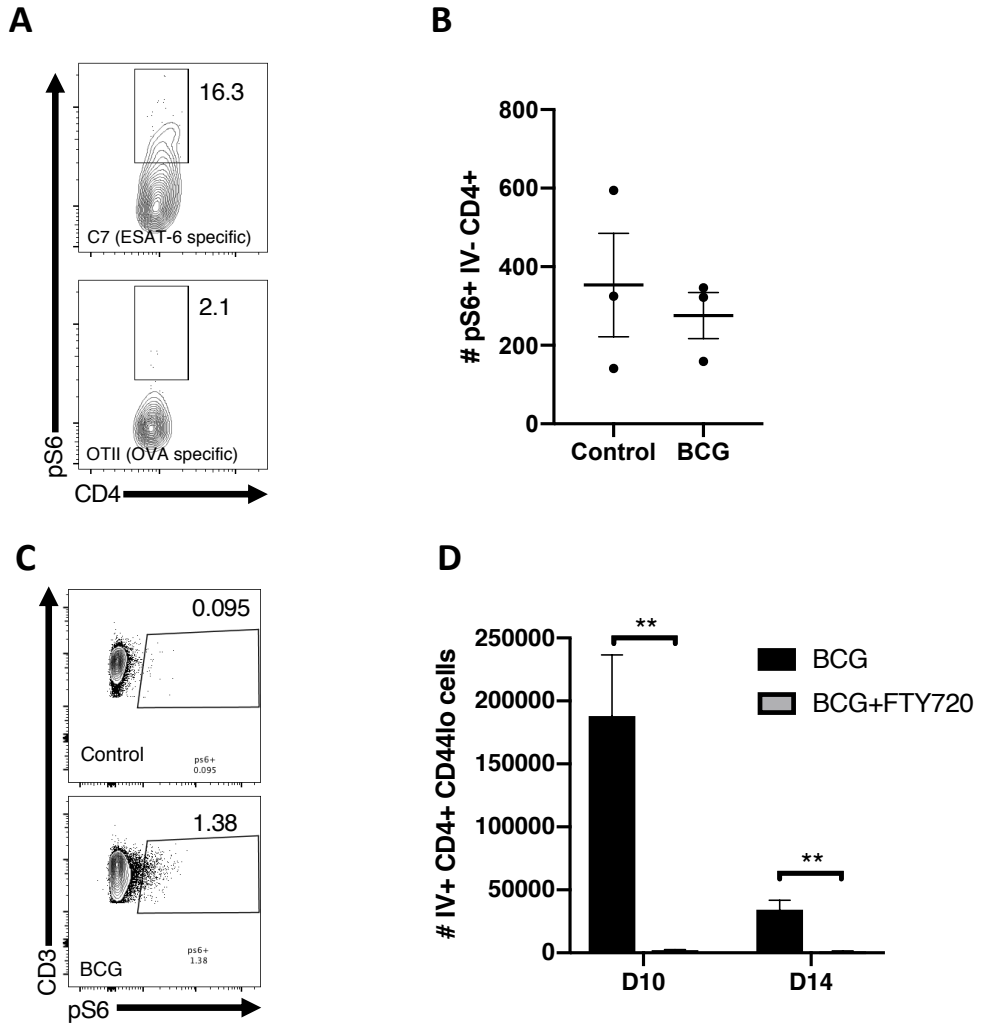

Supplemental Figure 2: pS6 as a marker of TCR stimulation.
(A) Mtb-specific C7 and OVA-specific OTII CD4 T cells were stimulated *in vitro* for 5d to generate Th1 cells. These were then co-transferred into D35 Mtb-infected animals. Quantitative histocytometry was used to determine pS6+ C7 and OTII cells. (B) Flow cytometry quantification of the number of i.v.- pS6+ CD4 T cells in mice prior to Mtb infection. (C) Representative flow plots of pS6 expression in lung T cells at D14. These plots are gated on i.v.- CD4+ cells. (D) Quantification of the number of i.v.+ CD4+ CD44lo cells in the lungs of Mtb-infected, BCG immunized animals that did or did not receive FTY720 treatment.

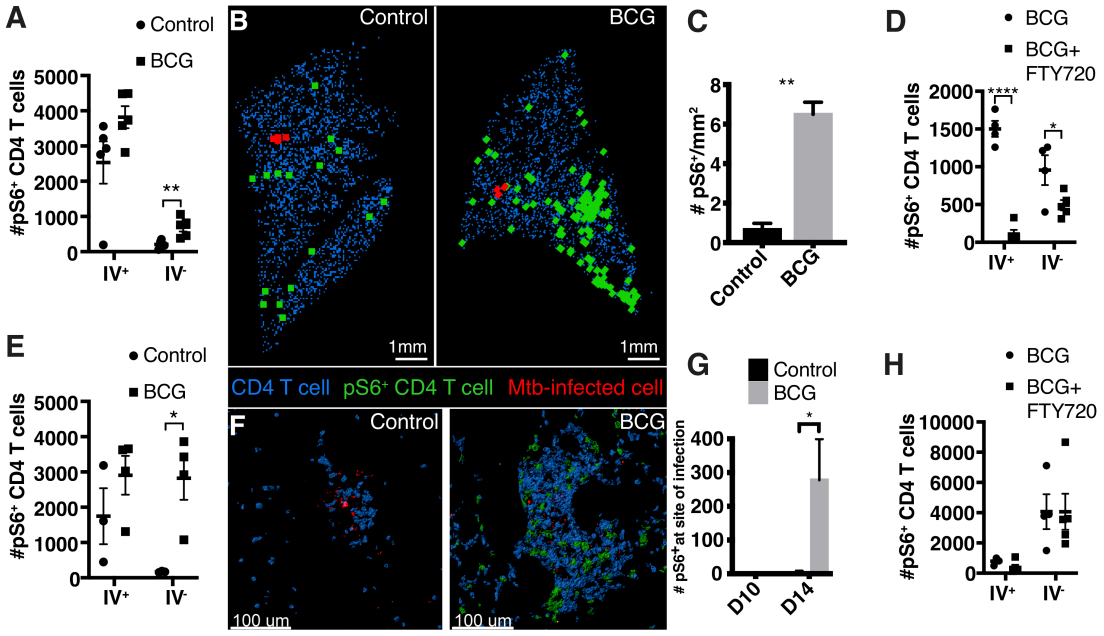

Figure 4: BCG-induced CD4 T cells are initially activated distal to the site of Mtb infection.
Total numbers of i.v.$^{+}$ and i.v.$^{-}$ pS6^{+} CD4 T cells at D10 (A) and D14 (E). Quantitative histocytometry was used to identify the location of CD4 T cells (blue) and pS6^{+} CD4 T cells (green) relative to infected cells (red) in lung sections at D10 (B) and sites of infection at D14 (F). (C) Number of pS6^{+} CD4 T cells per mm^{2} of lung at D10 as determined by quantitative histocytometry (n=2-3 mice/group). Total numbers of i.v.$^{+}$ and i.v.$^{-}$ pS6^{+} CD4 T cells at D10 (D) and D14 (H) in immunized mice treated with FTY720. (G) Number of pS6^{+} CD4 T cells within 80 μm of an infected cell (n=6-8 sections from 2 mice/group). This cutoff was based on the limit of IFNγ diffusion within tissue (128). Single-group comparisons were performed by unpaired t test. Data are presented as mean ± SEM. *p < 0.05, **p < 0.01.

In order to assess the intrapulmonary location of these pS6^{+} cells, we performed confocal imaging and quantitative histocytometry (Supplemental Fig. 3). Consistent with our flow cytometry data, there were significantly more pS6^{+} cells in lung sections from immunized mice at D10 (Fig. 4B-C), but surprisingly, few of these cells were located near infected cells (Fig. 4B, G). Thus, although BCG induces early T cell recruitment and activation, at D10 this occurs primarily in uninfected areas of the lung. This may be due to Mtb antigen export from infected to uninfected antigen-presenting cells (129), but could represent T cells that have recently trafficked from the lymph node (LN). To address this, we treated mice with FTY720, which blocks lymphocyte egress from lymphatic tissue, for 48 hours prior to analysis (Supplemental

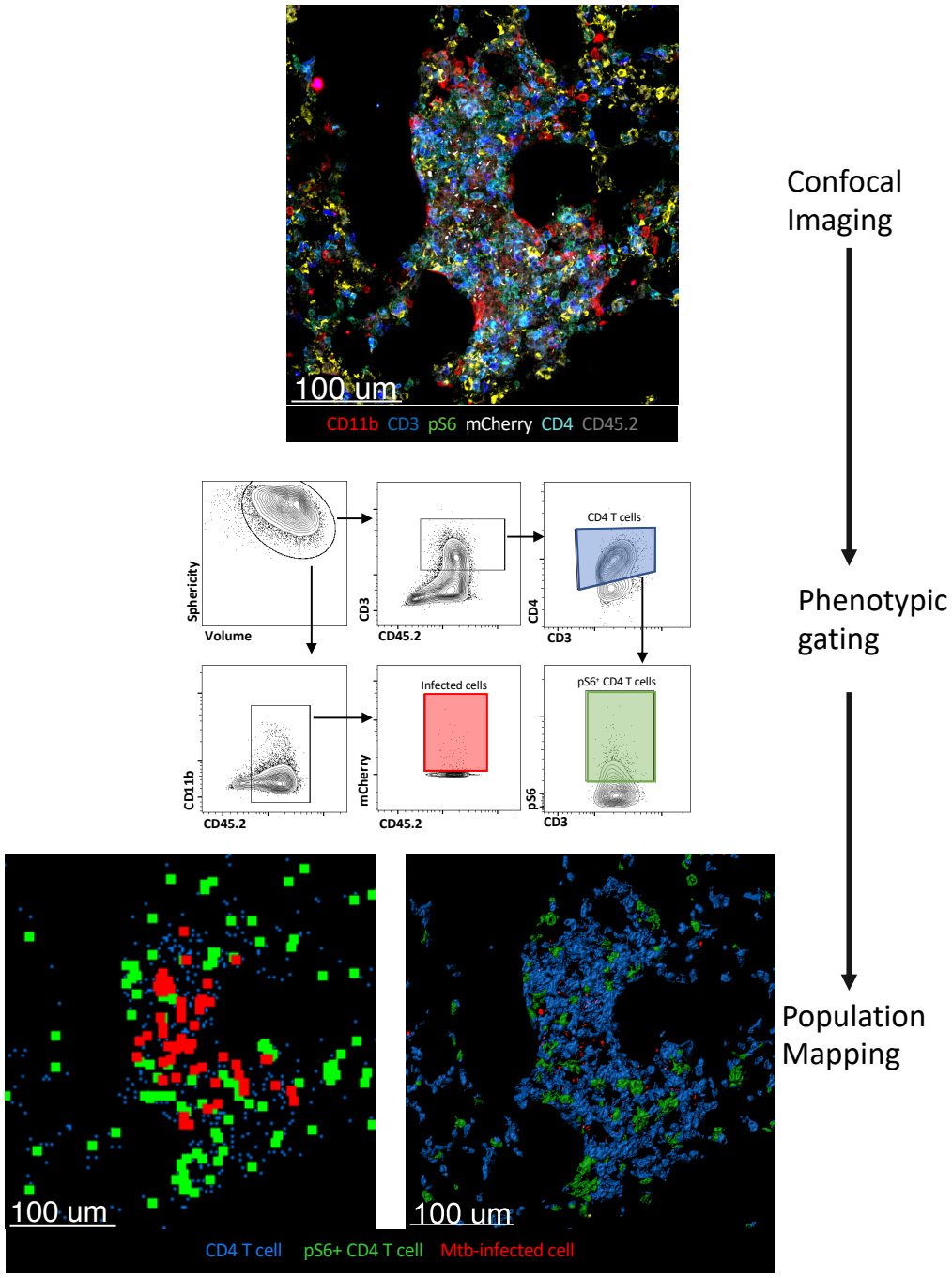

Supplemental Figure 3: Description of quantitative histocytometry analysis
A representative confocal image, histocytometry plots, and representative positional mapping are displayed. To perform this analysis, 20µm lung sections were stained with fluorescently-labeled antibodies and imaged with 12 parameter confocal microscopy. Surface objects are formed around each individual cell in Imaris (Bitplane), then exported into FlowJo. Gating of complex cell populations is completed using retained fluorescence data for each cell. Using retained positional data, cell types can be visualized in three-dimensional space. Overall, this allows us to achieve flow cytometry-like capacity to discriminate various cell subsets using their phenotypic and functional properties, while retaining information on their precise positioning within tissues. The population mapping is displayed both as dots indicating the position of gated cell objects (bottom left), and as shaded cell objects (bottom right). More detailed information can be found in Gerner et al., 2012 (88).

Fig. 2D). Although FTY720 treatment almost completely eliminated pS6$^+$ CD4 T cells in the lung vasculature at D10, the number of pS6$^+$ T cells in the lung parenchyma (iv$^-$) was only partially reduced (Fig. 4D).These results suggest that most of the recently activated T cells in the vasculature and a subset of those in the lung parenchyma had recently egressed from the lymph node. However, some of the pS6$^+$ cells in the lung parenchyma at D10 were likely activated in the lungs. Taken together, the activation of BCG-induced CD4 T cells, which occurs distal to sites of infection, shapes immunity to Mtb challenge earlier than previously appreciated by facilitating the pulmonary recruitment of MDM and accelerating the transfer of Mtb from AM to other myeloid cells. This transfer likely influences the ability of the BCG-immunized host to control Mtb, as prior studies have shown that tissue-resident vs. recruited macrophages differ profoundly in their capacity to control Mtb replication (46, 58). Future studies are needed to elucidate the overall impact on protection because the settings in which distinct macrophage types mediate enhanced immunity remain unclear.

Interestingly, BCG-induced CD4 T cells only begin to curb Mtb replication at D14, when they finally co-localize with cells harboring Mtb, as evidenced by the identification of many pS6$^+$ cells in the lung parenchyma and at sites of infection compared to controls (Fig. 4E-G). This is consistent with the finding that optimal immunity against Mtb requires direct interactions between antigen-specific CD4 T cells and infected cells (100). Importantly, in contrast to our findings at D10, at D14 FTY720 had no effect on the number of pS6$^+$ CD4 T cells recovered from the lung parenchyma of BCG-immunized mice (Fig. 4H), suggesting that almost all of these T cells were activated in the lungs rather than the lymph node. Why do T cells and Mtb-infected cells not co-localize earlier? The AM is the first cell type to become infected and remains the primary infected cell type for at least a week (45). During this time, the immune

system appears largely unaware of the looming threat, as few MDM or PMN are recruited to the lung. The recent finding that AM infection is non-inflammatory and poorly induces chemokines may help explain the covert nature of early infection (53). Identifying vaccination approaches that enable T cells to co-localize with Mtb-infected AM may promote earlier Mtb control. Together, these results demonstrate that BCG immunization shapes early T cell and myeloid cell responses in the lung and new vaccine strategies should consider the dynamics of both these compartments.

SUMMARY

Our findings provide new insight into the early immune response to Mtb infection. In Chapter 3, we perform a comparative analysis of alveolar and monocyte-derived macrophages, which are both targeted for infection. Here, we find that MDM robustly engage antibacterial response programs, and are a more protective cell type than AM, which upregulate proliferation and metabolic programs. In addition, we find that bacteria in MDM have a signature of hypoxic stress. These studies suggest that the AM may represent an attractive target for immunomodulation in order to shift this cell type towards a more protective response. In Chapter 4, we demonstrate how BCG immunization alters the cell types targeted for early Mtb infection. Immunization induces a population of lung-resident CD4 T cells, which are present prior to Mtb challenge, and are required for the more rapid transfer of bacteria from AM to lung-infiltrating phagocytes. By assessing the location of T cell activation within the lung, we find that T cell recognition of Mtb is initiated distal to the site of infection and precedes vaccine-induced protection. Our findings suggest that delayed co-localization of T cells and infected macrophages during the early stages of pulmonary infection represents an important barrier to protective immunity. Together, these findings have the potential to guide future rationale vaccine design to better control TB.

REFERENCES

1. Brites, D., and S. Gagneux. 2015. Co-evolution of Mycobacterium tuberculosis and Homo sapiens. *Immunol Rev* 264: 6-24.
2. World Health Organization. 2018. *Global tuberculosis report 2018*. World Health Organization, Geneva.
3. Murray, J. F., D. E. Schraufnagel, and P. C. Hopewell. 2015. Treatment of Tuberculosis. A Historical Perspective. *Ann Am Thorac Soc* 12: 1749-1759.
4. Benatar, S. R., and R. Upshur. 2010. Tuberculosis and poverty: what could (and should) be done? *Int J Tuberc Lung Dis* 14: 1215-1221.
5. Bottai, D., T. P. Stinear, P. Supply, and R. Brosch. 2014. Mycobacterial Pathogenomics and Evolution. *Microbiol Spectr* 2: MGM2-0025-2013.
6. Thoen, C., P. Lobue, and I. de Kantor. 2006. The importance of Mycobacterium bovis as a zoonosis. *Vet Microbiol* 112: 339-345.
7. Ramakrishnan, L. 2013. Looking Within the Zebrafish to Understand the Tuberculous Granuloma. In *The New Paradigm of Immunity to Tuberculosis*. M. Divangahi, ed. Springer New York, New York, NY. 251-266.
8. Hett, E. C., and E. J. Rubin. 2008. Bacterial growth and cell division: a mycobacterial perspective. *Microbiol Mol Biol Rev* 72: 126-156, table of contents.
9. Behr, M. A., P. H. Edelstein, and L. Ramakrishnan. 2018. Revisiting the timetable of tuberculosis. *BMJ* 362: k2738.
10. Toman, K. 2004. *Toman's tuberculosis : case detection, treatment, and monitoring : questions and answers*. Geneva : World Health Organization, Geneva.
11. Steingart, K. R., H. Sohn, I. Schiller, L. A. Kloda, C. C. Boehme, M. Pai, and N. Dendukuri. 2013. Xpert(R) MTB/RIF assay for pulmonary tuberculosis and rifampicin resistance in adults. *Cochrane Database Syst Rev*: CD009593.
12. Albert, H., R. R. Nathavitharana, C. Isaacs, M. Pai, C. M. Denkinger, and C. C. Boehme. 2016. Development, roll-out and impact of Xpert MTB/RIF for tuberculosis: what lessons have we learnt and how can we do better? *Eur Respir J* 48: 516-525.
13. Mazurek, G. H., M. E. Villarino, and Cdc. 2003. Guidelines for using the QuantiFERON-TB test for diagnosing latent Mycobacterium tuberculosis infection. Centers for Disease Control and Prevention. *MMWR Recomm Rep* 52: 15-18.
14. Pai, M., M. A. Behr, D. Dowdy, K. Dheda, M. Divangahi, C. C. Boehme, A. Ginsberg, S. Swaminathan, M. Spigelman, H. Getahun, D. Menzies, and M. Raviglione. 2016. Tuberculosis. *Nat Rev Dis Primers* 2: 16076.
15. Zak, D. E., A. Penn-Nicholson, T. J. Scriba, E. Thompson, S. Suliman, L. M. Amon, H. Mahomed, M. Erasmus, W. Whatney, G. D. Hussey, D. Abrahams, F. Kafaar, T. Hawkridge, S. Verver, E. J. Hughes, M. Ota, J. Sutherland, R. Howe, H. M. Dockrell, W. H. Boom, B. Thiel, T. H. M. Ottenhoff, H. Mayanja-Kizza, A. C. Crampin, K. Downing, M. Hatherill, J. Valvo, S. Shankar, S. K. Parida, S. H. E. Kaufmann, G. Walzl, A. Aderem, W. A. Hanekom, Acs, and G. C. c. s. groups. 2016. A blood RNA signature for tuberculosis disease risk: a prospective cohort study. *Lancet* 387: 2312-2322.
16. Lu, L. L., A. W. Chung, T. R. Rosebrock, M. Ghebremichael, W. H. Yu, P. S. Grace, M. K. Schoen, F. Tafesse, C. Martin, V. Leung, A. E. Mahan, M. Sips, M. P. Kumar, J. Tedesco, H. Robinson, E. Tkachenko, M. Draghi, K. J. Freedberg, H. Streeck, T. J.

Suscovich, D. A. Lauffenburger, B. I. Restrepo, C. Day, S. M. Fortune, and G. Alter. 2016. A Functional Role for Antibodies in Tuberculosis. *Cell* 167: 433-443 e414.
17. Behr, M. A., M. A. Wilson, W. P. Gill, H. Salamon, G. K. Schoolnik, S. Rane, and P. M. Small. 1999. Comparative genomics of BCG vaccines by whole-genome DNA microarray. *Science* 284: 1520-1523.
18. Lewis, K. N., R. Liao, K. M. Guinn, M. J. Hickey, S. Smith, M. A. Behr, and D. R. Sherman. 2003. Deletion of RD1 from Mycobacterium tuberculosis mimics bacille Calmette-Guerin attenuation. *J Infect Dis* 187: 117-123.
19. Mangtani, P., I. Abubakar, C. Ariti, R. Beynon, L. Pimpin, P. E. Fine, L. C. Rodrigues, P. G. Smith, M. Lipman, P. F. Whiting, and J. A. Sterne. 2014. Protection by BCG vaccine against tuberculosis: a systematic review of randomized controlled trials. *Clin Infect Dis* 58: 470-480.
20. Poyntz, H. C., E. Stylianou, K. L. Griffiths, L. Marsay, A. M. Checkley, and H. McShane. 2014. Non-tuberculous mycobacteria have diverse effects on BCG efficacy against Mycobacterium tuberculosis. *Tuberculosis (Edinb)* 94: 226-237.
21. Palmer, C. E., and M. W. Long. 1966. Effects of infection with atypical mycobacteria on BCG vaccination and tuberculosis. *Am Rev Respir Dis* 94: 553-568.
22. Morales, A., D. Eidinger, and A. W. Bruce. 1976. Intracavitary Bacillus Calmette-Guerin in the treatment of superficial bladder tumors. *J Urol* 116: 180-183.
23. Aaby, P., A. Roth, H. Ravn, B. M. Napirna, A. Rodrigues, I. M. Lisse, L. Stensballe, B. R. Diness, K. R. Lausch, N. Lund, S. Biering-Sorensen, H. Whittle, and C. S. Benn. 2011. Randomized trial of BCG vaccination at birth to low-birth-weight children: beneficial nonspecific effects in the neonatal period? *J Infect Dis* 204: 245-252.
24. Kaufmann, E., J. Sanz, J. L. Dunn, N. Khan, L. E. Mendonca, A. Pacis, F. Tzelepis, E. Pernet, A. Dumaine, J. C. Grenier, F. Mailhot-Leonard, E. Ahmed, J. Belle, R. Besla, B. Mazer, I. L. King, A. Nijnik, C. S. Robbins, L. B. Barreiro, and M. Divangahi. 2018. BCG Educates Hematopoietic Stem Cells to Generate Protective Innate Immunity against Tuberculosis. *Cell* 172: 176-190 e119.
25. Butkeviciute, E., C. E. Jones, and S. G. Smith. 2018. Heterologous effects of infant BCG vaccination: potential mechanisms of immunity. *Future Microbiol* 13: 1193-1208.
26. Roth, A. E., L. G. Stensballe, M. L. Garly, and P. Aaby. 2006. Beneficial non-targeted effects of BCG--ethical implications for the coming introduction of new TB vaccines. *Tuberculosis (Edinb)* 86: 397-403.
27. Van Der Meeren, O., M. Hatherill, V. Nduba, R. J. Wilkinson, M. Muyoyeta, E. Van Brakel, H. M. Ayles, G. Henostroza, F. Thienemann, T. J. Scriba, A. Diacon, G. L. Blatner, M. A. Demoitie, M. Tameris, M. Malahleha, J. C. Innes, E. Hellstrom, N. Martinson, T. Singh, E. J. Akite, A. Khatoon Azam, A. Bollaerts, A. M. Ginsberg, T. G. Evans, P. Gillard, and D. R. Tait. 2018. Phase 2b Controlled Trial of M72/AS01E Vaccine to Prevent Tuberculosis. *N Engl J Med* 379: 1621-1634.
28. Iseman, M. D. 2002. Tuberculosis therapy: past, present and future. *Eur Respir J Suppl* 36: 87s-94s.
29. 1950. TREATMENT of pulmonary tuberculosis with streptomycin and para-aminosalicylic acid; a Medical Research Council investigation. *Br Med J* 2: 1073-1085.
30. Turnbull, F. W., A. T. Wallace, S. Stewart, and J. W. Crofton. 1953. Streptomycin resistance in patients with pulmonary tuberculosis previously treated with P.A.S. alone. *Br Med J* 1: 1244-1246.

31. Organization, W. H. 2017. Guidelines for treatment of drug-susceptible tuberculosis and patient care.
32. Hussell, T., and T. J. Bell. 2014. Alveolar macrophages: plasticity in a tissue-specific context. *Nat Rev Immunol* 14: 81-93.
33. Guilliams, M., I. De Kleer, S. Henri, S. Post, L. Vanhoutte, S. De Prijck, K. Deswarte, B. Malissen, H. Hammad, and B. N. Lambrecht. 2013. Alveolar macrophages develop from fetal monocytes that differentiate into long-lived cells in the first week of life via GM-CSF. *J Exp Med* 210: 1977-1992.
34. Hashimoto, D., A. Chow, C. Noizat, P. Teo, M. B. Beasley, M. Leboeuf, C. D. Becker, P. See, J. Price, D. Lucas, M. Greter, A. Mortha, S. W. Boyer, E. C. Forsberg, M. Tanaka, N. van Rooijen, A. Garcia-Sastre, E. R. Stanley, F. Ginhoux, P. S. Frenette, and M. Merad. 2013. Tissue-resident macrophages self-maintain locally throughout adult life with minimal contribution from circulating monocytes. *Immunity* 38: 792-804.
35. Baker, A. D., A. Malur, B. P. Barna, S. Ghosh, M. S. Kavuru, A. G. Malur, and M. J. Thomassen. 2010. Targeted PPAR{gamma} deficiency in alveolar macrophages disrupts surfactant catabolism. *J Lipid Res* 51: 1325-1331.
36. Kumar, A., B. Abdelmalak, Y. Inoue, and D. A. Culver. 2018. Pulmonary alveolar proteinosis in adults: pathophysiology and clinical approach. *Lancet Respir Med* 6: 554-565.
37. Stanley, E., G. J. Lieschke, D. Grail, D. Metcalf, G. Hodgson, J. A. Gall, D. W. Maher, J. Cebon, V. Sinickas, and A. R. Dunn. 1994. Granulocyte/macrophage colony-stimulating factor-deficient mice show no major perturbation of hematopoiesis but develop a characteristic pulmonary pathology. *Proc Natl Acad Sci U S A* 91: 5592-5596.
38. Knapp, S., J. C. Leemans, S. Florquin, J. Branger, N. A. Maris, J. Pater, N. van Rooijen, and T. van der Poll. 2003. Alveolar macrophages have a protective antiinflammatory role during murine pneumococcal pneumonia. *Am J Respir Crit Care Med* 167: 171-179.
39. Broug-Holub, E., G. B. Toews, J. F. van Iwaarden, R. M. Strieter, S. L. Kunkel, R. Paine, 3rd, and T. J. Standiford. 1997. Alveolar macrophages are required for protective pulmonary defenses in murine Klebsiella pneumonia: elimination of alveolar macrophages increases neutrophil recruitment but decreases bacterial clearance and survival. *Infect Immun* 65: 1139-1146.
40. Kolli, D., M. R. Gupta, E. Sbrana, T. S. Velayutham, H. Chao, A. Casola, and R. P. Garofalo. 2014. Alveolar macrophages contribute to the pathogenesis of human metapneumovirus infection while protecting against respiratory syncytial virus infection. *Am J Respir Cell Mol Biol* 51: 502-515.
41. Schneider, C., S. P. Nobs, A. K. Heer, M. Kurrer, G. Klinke, N. van Rooijen, J. Vogel, and M. Kopf. 2014. Alveolar macrophages are essential for protection from respiratory failure and associated morbidity following influenza virus infection. *PLoS Pathog* 10: e1004053.
42. Lauzon-Joset, J. F., D. Marsolais, A. Langlois, and E. Y. Bissonnette. 2014. Dysregulation of alveolar macrophages unleashes dendritic cell-mediated mechanisms of allergic airway inflammation. *Mucosal Immunol* 7: 155-164.
43. Kopf, M., C. Schneider, and S. P. Nobs. 2015. The development and function of lung-resident macrophages and dendritic cells. *Nat Immunol* 16: 36-44.
44. Gautier, E. L., A. Chow, R. Spanbroek, G. Marcelin, M. Greter, C. Jakubzick, M. Bogunovic, M. Leboeuf, N. van Rooijen, A. J. Habenicht, M. Merad, and G. J. Randolph.

2012. Systemic analysis of PPARgamma in mouse macrophage populations reveals marked diversity in expression with critical roles in resolution of inflammation and airway immunity. *J Immunol* 189: 2614-2624.

45. Cohen, S. B., B. H. Gern, J. L. Delahaye, K. N. Adams, C. R. Plumlee, J. K. Winkler, D. R. Sherman, M. Y. Gerner, and K. B. Urdahl. 2018. Alveolar Macrophages Provide an Early Mycobacterium tuberculosis Niche and Initiate Dissemination. *Cell Host Microbe* 24: 439-446 e434.
46. Huang, L., E. V. Nazarova, S. Tan, Y. Liu, and D. G. Russell. 2018. Growth of Mycobacterium tuberculosis in vivo segregates with host macrophage metabolism and ontogeny. *J Exp Med* 215: 1135-1152.
47. Rothchild, A. C., G. S. Olson, J. Nemeth, L. M. Amon, D. Mai, E. S. Gold, A. H. Diercks, and A. Aderem. 2019. Alveolar macrophages up-regulate a non-classical innate response to Mycobacterium tuberculosis infection in vivo. *bioRxiv*: 520791.
48. Devi, S., Y. Wang, W. K. Chew, R. Lima, A. G. N, C. N. Mattar, S. Z. Chong, A. Schlitzer, N. Bakocevic, S. Chew, J. L. Keeble, C. C. Goh, J. L. Li, M. Evrard, B. Malleret, A. Larbi, L. Renia, M. Haniffa, S. M. Tan, J. K. Chan, K. Balabanian, T. Nagasawa, F. Bachelerie, A. Hidalgo, F. Ginhoux, P. Kubes, and L. G. Ng. 2013. Neutrophil mobilization via plerixafor-mediated CXCR4 inhibition arises from lung demargination and blockade of neutrophil homing to the bone marrow. *J Exp Med* 210: 2321-2336.
49. Yang, C. T., C. J. Cambier, J. M. Davis, C. J. Hall, P. S. Crosier, and L. Ramakrishnan. 2012. Neutrophils exert protection in the early tuberculous granuloma by oxidative killing of mycobacteria phagocytosed from infected macrophages. *Cell Host Microbe* 12: 301-312.
50. Kimmey, J. M., J. P. Huynh, L. A. Weiss, S. Park, A. Kambal, J. Debnath, H. W. Virgin, and C. L. Stallings. 2015. Unique role for ATG5 in neutrophil-mediated immunopathology during M. tuberculosis infection. *Nature* 528: 565-569.
51. Dallenga, T., U. Repnik, B. Corleis, J. Eich, R. Reimer, G. W. Griffiths, and U. E. Schaible. 2017. M. tuberculosis-Induced Necrosis of Infected Neutrophils Promotes Bacterial Growth Following Phagocytosis by Macrophages. *Cell Host Microbe* 22: 519-530 e513.
52. Mishra, B. B., R. R. Lovewell, A. J. Olive, G. Zhang, W. Wang, E. Eugenin, C. M. Smith, J. Y. Phuah, J. E. Long, M. L. Dubuke, S. G. Palace, J. D. Goguen, R. E. Baker, S. Nambi, R. Mishra, M. G. Booty, C. E. Baer, S. A. Shaffer, V. Dartois, B. A. McCormick, X. Chen, and C. M. Sassetti. 2017. Nitric oxide prevents a pathogen-permissive granulocytic inflammation during tuberculosis. *Nat Microbiol* 2: 17072.
53. Rothchild, A. C., G. S. Olson, J. Nemeth, L. M. Amon, D. Mai, E. S. Gold, A. H. Diercks, and A. Aderem. 2019. Alveolar macrophages generate a non-canonical NRF2-driven transcriptional response to *Mycobacterium tuberculosis in vivo*. *Sci Immunol*.
54. Wolf, A. J., B. Linas, G. J. Trevejo-Nunez, E. Kincaid, T. Tamura, K. Takatsu, and J. D. Ernst. 2007. Mycobacterium tuberculosis infects dendritic cells with high frequency and impairs their function in vivo. *J Immunol* 179: 2509-2519.
55. Guilliams, M., C. A. Dutertre, C. L. Scott, N. McGovern, D. Sichien, S. Chakarov, S. Van Gassen, J. Chen, M. Poidinger, S. De Prijck, S. J. Tavernier, I. Low, S. E. Irac, C. N. Mattar, H. R. Sumatoh, G. H. L. Low, T. J. K. Chung, D. K. H. Chan, K. K. Tan, T. L. K. Hon, E. Fossum, B. Bogen, M. Choolani, J. K. Y. Chan, A. Larbi, H. Luche, S. Henri, Y.

Saeys, E. W. Newell, B. N. Lambrecht, B. Malissen, and F. Ginhoux. 2016. Unsupervised High-Dimensional Analysis Aligns Dendritic Cells across Tissues and Species. *Immunity* 45: 669-684.
56. Min, J., D. Yang, M. Kim, K. Haam, A. Yoo, J. H. Choi, B. U. Schraml, Y. S. Kim, D. Kim, and S. J. Kang. 2018. Inflammation induces two types of inflammatory dendritic cells in inflamed lymph nodes. *Exp Mol Med* 50: e458.
57. Cambier, C. J., S. M. O'Leary, M. P. O'Sullivan, J. Keane, and L. Ramakrishnan. 2017. Phenolic Glycolipid Facilitates Mycobacterial Escape from Microbicidal Tissue-Resident Macrophages. *Immunity* 47: 552-565 e554.
58. Cambier, C. J., K. K. Takaki, R. P. Larson, R. E. Hernandez, D. M. Tobin, K. B. Urdahl, C. L. Cosma, and L. Ramakrishnan. 2014. Mycobacteria manipulate macrophage recruitment through coordinated use of membrane lipids. *Nature* 505: 218-222.
59. Samstein, M., H. A. Schreiber, I. M. Leiner, B. Susac, M. S. Glickman, and E. G. Pamer. 2013. Essential yet limited role for CCR2(+) inflammatory monocytes during Mycobacterium tuberculosis-specific T cell priming. *Elife* 2: e01086.
60. Stamm, C. E., A. C. Collins, and M. U. Shiloh. 2015. Sensing of Mycobacterium tuberculosis and consequences to both host and bacillus. *Immunol Rev* 264: 204-219.
61. Fratti, R. A., J. M. Backer, J. Gruenberg, S. Corvera, and V. Deretic. 2001. Role of phosphatidylinositol 3-kinase and Rab5 effectors in phagosomal biogenesis and mycobacterial phagosome maturation arrest. *J Cell Biol* 154: 631-644.
62. Fratti, R. A., J. Chua, I. Vergne, and V. Deretic. 2003. Mycobacterium tuberculosis glycosylated phosphatidylinositol causes phagosome maturation arrest. *Proc Natl Acad Sci U S A* 100: 5437-5442.
63. Vergne, I., J. Chua, H. H. Lee, M. Lucas, J. Belisle, and V. Deretic. 2005. Mechanism of phagolysosome biogenesis block by viable Mycobacterium tuberculosis. *Proc Natl Acad Sci U S A* 102: 4033-4038.
64. Wong, K. W., and W. R. Jacobs, Jr. 2011. Critical role for NLRP3 in necrotic death triggered by Mycobacterium tuberculosis. *Cell Microbiol* 13: 1371-1384.
65. Simeone, R., F. Sayes, O. Song, M. I. Groschel, P. Brodin, R. Brosch, and L. Majlessi. 2015. Cytosolic access of Mycobacterium tuberculosis: critical impact of phagosomal acidification control and demonstration of occurrence in vivo. *PLoS Pathog* 11: e1004650.
66. Houben, D., C. Demangel, J. van Ingen, J. Perez, L. Baldeon, A. M. Abdallah, L. Caleechurn, D. Bottai, M. van Zon, K. de Punder, T. van der Laan, A. Kant, R. Bossers-de Vries, P. Willemsen, W. Bitter, D. van Soolingen, R. Brosch, N. van der Wel, and P. J. Peters. 2012. ESX-1-mediated translocation to the cytosol controls virulence of mycobacteria. *Cell Microbiol* 14: 1287-1298.
67. Augenstreich, J., A. Arbues, R. Simeone, E. Haanappel, A. Wegener, F. Sayes, F. Le Chevalier, C. Chalut, W. Malaga, C. Guilhot, R. Brosch, and C. Astarie-Dequeker. 2017. ESX-1 and phthiocerol dimycocerosates of Mycobacterium tuberculosis act in concert to cause phagosomal rupture and host cell apoptosis. *Cell Microbiol* 19.
68. Collins, A. C., H. Cai, T. Li, L. H. Franco, X. D. Li, V. R. Nair, C. R. Scharn, C. E. Stamm, B. Levine, Z. J. Chen, and M. U. Shiloh. 2015. Cyclic GMP-AMP Synthase Is an Innate Immune DNA Sensor for Mycobacterium tuberculosis. *Cell Host Microbe* 17: 820-828.

69. Wassermann, R., M. F. Gulen, C. Sala, S. G. Perin, Y. Lou, J. Rybniker, J. L. Schmid-Burgk, T. Schmidt, V. Hornung, S. T. Cole, and A. Ablasser. 2015. Mycobacterium tuberculosis Differentially Activates cGAS- and Inflammasome-Dependent Intracellular Immune Responses through ESX-1. *Cell Host Microbe* 17: 799-810.
70. Watson, R. O., S. L. Bell, D. A. MacDuff, J. M. Kimmey, E. J. Diner, J. Olivas, R. E. Vance, C. L. Stallings, H. W. Virgin, and J. S. Cox. 2015. The Cytosolic Sensor cGAS Detects Mycobacterium tuberculosis DNA to Induce Type I Interferons and Activate Autophagy. *Cell Host Microbe* 17: 811-819.
71. Dorhoi, A., V. Yeremeev, G. Nouailles, J. Weiner, 3rd, S. Jorg, E. Heinemann, D. Oberbeck-Muller, J. K. Knaul, A. Vogelzang, S. T. Reece, K. Hahnke, H. J. Mollenkopf, V. Brinkmann, and S. H. Kaufmann. 2014. Type I IFN signaling triggers immunopathology in tuberculosis-susceptible mice by modulating lung phagocyte dynamics. *Eur J Immunol* 44: 2380-2393.
72. Watson, R. O., P. S. Manzanillo, and J. S. Cox. 2012. Extracellular M. tuberculosis DNA targets bacteria for autophagy by activating the host DNA-sensing pathway. *Cell* 150: 803-815.
73. Deffur, A., N. J. Mulder, and R. J. Wilkinson. 2013. Co-infection with Mycobacterium tuberculosis and human immunodeficiency virus: an overview and motivation for systems approaches. *Pathog Dis* 69: 101-113.
74. Cooper, A. M. 2009. Cell-mediated immune responses in tuberculosis. *Annu Rev Immunol* 27: 393-422.
75. Urdahl, K. B., S. Shafiani, and J. D. Ernst. 2011. Initiation and regulation of T-cell responses in tuberculosis. *Mucosal Immunol* 4: 288-293.
76. Wolf, A. J., L. Desvignes, B. Linas, N. Banaiee, T. Tamura, K. Takatsu, and J. D. Ernst. 2008. Initiation of the adaptive immune response to Mycobacterium tuberculosis depends on antigen production in the local lymph node, not the lungs. *J Exp Med* 205: 105-115.
77. Reiley, W. W., M. D. Calayag, S. T. Wittmer, J. L. Huntington, J. E. Pearl, J. J. Fountain, C. A. Martino, A. D. Roberts, A. M. Cooper, G. M. Winslow, and D. L. Woodland. 2008. ESAT-6-specific CD4 T cell responses to aerosol Mycobacterium tuberculosis infection are initiated in the mediastinal lymph nodes. *Proc Natl Acad Sci U S A* 105: 10961-10966.
78. Wallgren, A. 1948. The time-table of tuberculosis. *Tubercle* 29: 245-251.
79. Poulsen, A. 1950. Some clinical features of tuberculosis. 1. Incubation period. *Acta Tuberc Scand* 24: 311-346.
80. Shafiani, S., G. Tucker-Heard, A. Kariyone, K. Takatsu, and K. B. Urdahl. 2010. Pathogen-specific regulatory T cells delay the arrival of effector T cells in the lung during early tuberculosis. *J Exp Med* 207: 1409-1420.
81. Shafiani, S., C. Dinh, J. M. Ertelt, A. O. Moguche, I. Siddiqui, K. S. Smigiel, P. Sharma, D. J. Campbell, S. S. Way, and K. B. Urdahl. 2013. Pathogen-specific Treg cells expand early during mycobacterium tuberculosis infection but are later eliminated in response to Interleukin-12. *Immunity* 38: 1261-1270.
82. Monin, L., K. L. Griffiths, S. Slight, Y. Lin, J. Rangel-Moreno, and S. A. Khader. 2015. Immune requirements for protective Th17 recall responses to Mycobacterium tuberculosis challenge. *Mucosal Immunol* 8: 1099-1109.
83. Sallin, M. A., K. D. Kauffman, C. Riou, E. Du Bruyn, T. W. Foreman, S. Sakai, S. G. Hoft, T. G. Myers, P. J. Gardina, A. Sher, R. Moore, T. Wilder-Kofie, I. N. Moore, A.

Sette, C. S. Lindestam Arlehamn, R. J. Wilkinson, and D. L. Barber. 2018. Host resistance to pulmonary Mycobacterium tuberculosis infection requires CD153 expression. *Nat Microbiol* 3: 1198-1205.
84. McLane, L. M., M. S. Abdel-Hakeem, and E. J. Wherry. 2019. CD8 T Cell Exhaustion During Chronic Viral Infection and Cancer. *Annu Rev Immunol* 37: 457-495.
85. Moguche, A. O., M. Musvosvi, A. Penn-Nicholson, C. R. Plumlee, H. Mearns, H. Geldenhuys, E. Smit, D. Abrahams, V. Rozot, O. Dintwe, S. T. Hoff, I. Kromann, M. Ruhwald, P. Bang, R. P. Larson, S. Shafiani, S. Ma, D. R. Sherman, A. Sette, C. S. Lindestam Arlehamn, D. M. McKinney, H. Maecker, W. A. Hanekom, M. Hatherill, P. Andersen, T. J. Scriba, and K. B. Urdahl. 2017. Antigen Availability Shapes T Cell Differentiation and Function during Tuberculosis. *Cell Host Microbe* 21: 695-706 e695.
86. Gallegos, A. M., E. G. Pamer, and M. S. Glickman. 2008. Delayed protection by ESAT-6-specific effector CD4+ T cells after airborne M. tuberculosis infection. *J Exp Med* 205: 2359-2368.
87. Cosma, C. L., O. Humbert, and L. Ramakrishnan. 2004. Superinfecting mycobacteria home to established tuberculous granulomas. *Nat Immunol* 5: 828-835.
88. Gerner, M. Y., W. Kastenmuller, I. Ifrim, J. Kabat, and R. N. Germain. 2012. Histo-cytometry: a method for highly multiplex quantitative tissue imaging analysis applied to dendritic cell subset microanatomy in lymph nodes. *Immunity* 37: 364-376.
89. Love, M. I., W. Huber, and S. Anders. 2014. Moderated estimation of fold change and dispersion for RNA-seq data with DESeq2. *Genome Biol* 15: 550.
90. Reiss, D. J., C. L. Plaisier, W. J. Wu, and N. S. Baliga. 2015. cMonkey2: Automated, systematic, integrated detection of co-regulated gene modules for any organism. *Nucleic Acids Res* 43: e87.
91. Peterson, E. J., R. Bailo, A. C. Rothchild, M. L. Arrieta-Ortiz, A. Kaur, M. Pan, D. Mai, A. A. Abidi, C. Cooper, A. Aderem, A. Bhatt, and N. S. Baliga. 2019. Path-seq identifies an essential mycolate remodeling program for mycobacterial host adaptation. *Mol Syst Biol* 15: e8584.
92. Breitling, R., P. Armengaud, A. Amtmann, and P. Herzyk. 2004. Rank products: a simple, yet powerful, new method to detect differentially regulated genes in replicated microarray experiments. *FEBS Lett* 573: 83-92.
93. Tusher, V. G., R. Tibshirani, and G. Chu. 2001. Significance analysis of microarrays applied to the ionizing radiation response. *Proc Natl Acad Sci U S A* 98: 5116-5121.
94. Robinson, M. D., and G. K. Smyth. 2008. Small-sample estimation of negative binomial dispersion, with applications to SAGE data. *Biostatistics* 9: 321-332.
95. Tameris, M. D., M. Hatherill, B. S. Landry, T. J. Scriba, M. A. Snowden, S. Lockhart, J. E. Shea, J. B. McClain, G. D. Hussey, W. A. Hanekom, H. Mahomed, H. McShane, and M. A. T. S. Team. 2013. Safety and efficacy of MVA85A, a new tuberculosis vaccine, in infants previously vaccinated with BCG: a randomised, placebo-controlled phase 2b trial. *Lancet* 381: 1021-1028.
96. Sakai, S., K. D. Kauffman, M. A. Sallin, A. H. Sharpe, H. A. Young, V. V. Ganusov, and D. L. Barber. 2016. CD4 T Cell-Derived IFN-gamma Plays a Minimal Role in Control of Pulmonary Mycobacterium tuberculosis Infection and Must Be Actively Repressed by PD-1 to Prevent Lethal Disease. *PLoS Pathog* 12: e1005667.

97. Anderson, K. G., K. Mayer-Barber, H. Sung, L. Beura, B. R. James, J. J. Taylor, L. Qunaj, T. S. Griffith, V. Vezys, D. L. Barber, and D. Masopust. 2014. Intravascular staining for discrimination of vascular and tissue leukocytes. *Nat Protoc* 9: 209-222.
98. Sakai, S., K. D. Kauffman, J. M. Schenkel, C. C. McBerry, K. D. Mayer-Barber, D. Masopust, and D. L. Barber. 2014. Cutting edge: control of Mycobacterium tuberculosis infection by a subset of lung parenchyma-homing CD4 T cells. *J Immunol* 192: 2965-2969.
99. Moguche, A. O., S. Shafiani, C. Clemons, R. P. Larson, C. Dinh, L. E. Higdon, C. J. Cambier, J. R. Sissons, A. M. Gallegos, P. J. Fink, and K. B. Urdahl. 2015. ICOS and Bcl6-dependent pathways maintain a CD4 T cell population with memory-like properties during tuberculosis. *J Exp Med* 212: 715-728.
100. Srivastava, S., and J. D. Ernst. 2013. Cutting edge: Direct recognition of infected cells by CD4 T cells is required for control of intracellular Mycobacterium tuberculosis in vivo. *J Immunol* 191: 1016-1020.
101. MacMicking, J. D., R. J. North, R. LaCourse, J. S. Mudgett, S. K. Shah, and C. F. Nathan. 1997. Identification of nitric oxide synthase as a protective locus against tuberculosis. *Proc Natl Acad Sci U S A* 94: 5243-5248.
102. Ranjbar, S., V. Haridas, L. D. Jasenosky, J. V. Falvo, and A. E. Goldfeld. 2015. A Role for IFITM Proteins in Restriction of Mycobacterium tuberculosis Infection. *Cell Rep* 13: 874-883.
103. Gardet, A., Y. Benita, C. Li, B. E. Sands, I. Ballester, C. Stevens, J. R. Korzenik, J. D. Rioux, M. J. Daly, R. J. Xavier, and D. K. Podolsky. 2010. LRRK2 is involved in the IFN-gamma response and host response to pathogens. *J Immunol* 185: 5577-5585.
104. Kim, K. S., P. C. Marcogliese, J. Yang, S. M. Callaghan, V. Resende, E. Abdel-Messih, C. Marras, N. P. Visanji, J. Huang, M. G. Schlossmacher, L. Trinkle-Mulcahy, R. S. Slack, A. E. Lang, T. Canadian Lrrk2 in Inflammation, and D. S. Park. 2018. Regulation of myeloid cell phagocytosis by LRRK2 via WAVE2 complex stabilization is altered in Parkinson's disease. *Proc Natl Acad Sci U S A* 115: E5164-E5173.
105. Wang, Z., S. Arat, M. Magid-Slav, and J. R. Brown. 2018. Meta-analysis of human gene expression in response to Mycobacterium tuberculosis infection reveals potential therapeutic targets. *BMC Syst Biol* 12: 3.
106. Hartlova, A., S. Herbst, J. Peltier, A. Rodgers, O. Bilkei-Gorzo, A. Fearns, B. D. Dill, H. Lee, R. Flynn, S. A. Cowley, P. Davies, P. A. Lewis, I. G. Ganley, J. Martinez, D. R. Alessi, A. D. Reith, M. Trost, and M. G. Gutierrez. 2018. LRRK2 is a negative regulator of Mycobacterium tuberculosis phagosome maturation in macrophages. *EMBO J* 37.
107. Braverman, J., K. M. Sogi, D. Benjamin, D. K. Nomura, and S. A. Stanley. 2016. HIF-1alpha Is an Essential Mediator of IFN-gamma-Dependent Immunity to Mycobacterium tuberculosis. *J Immunol* 197: 1287-1297.
108. Woods, S., J. Schroeder, H. A. McGachy, R. Plevin, C. W. Roberts, and J. Alexander. 2013. MAP kinase phosphatase-2 plays a key role in the control of infection with Toxoplasma gondii by modulating iNOS and arginase-1 activities in mice. *PLoS Pathog* 9: e1003535.
109. Al-Mutairi, M. S., L. C. Cadalbert, H. A. McGachy, M. Shweash, J. Schroeder, M. Kurnik, C. M. Sloss, C. E. Bryant, J. Alexander, and R. Plevin. 2010. MAP kinase phosphatase-2 plays a critical role in response to infection by Leishmania mexicana. *PLoS Pathog* 6: e1001192.

110. MacMicking, J., Q. W. Xie, and C. Nathan. 1997. Nitric oxide and macrophage function. *Annu Rev Immunol* 15: 323-350.
111. Sayin, V. I., A. Nilton, M. X. Ibrahim, P. Agren, E. Larsson, M. M. Petit, L. M. Hulten, M. Stahlman, B. R. Johansson, M. O. Bergo, and P. Lindahl. 2013. Zfp148 deficiency causes lung maturation defects and lethality in newborn mice that are rescued by deletion of p53 or antioxidant treatment. *PLoS One* 8: e55720.
112. Sayin, V. I., O. M. Khan, L. E. Pehlivanoglu, A. Staffas, M. X. Ibrahim, A. Asplund, P. Agren, A. Nilton, G. Bergstrom, M. O. Bergo, J. Boren, and P. Lindahl. 2014. Loss of one copy of Zfp148 reduces lesional macrophage proliferation and atherosclerosis in mice by activating p53. *Circ Res* 115: 781-789.
113. Chang, H., J. Song, J. Wu, and Y. Zhang. 2018. E2F transcription factor 8 promotes cell proliferation via CCND1/p21 in esophageal squamous cell carcinoma. *Onco Targets Ther* 11: 8165-8173.
114. Ye, L., L. Guo, Z. He, X. Wang, C. Lin, X. Zhang, S. Wu, Y. Bao, Q. Yang, L. Song, and H. Lin. 2016. Upregulation of E2F8 promotes cell proliferation and tumorigenicity in breast cancer by modulating G1/S phase transition. *Oncotarget* 7: 23757-23771.
115. Laub, F., R. Aldabe, V. Friedrich, Jr., S. Ohnishi, T. Yoshida, and F. Ramirez. 2001. Developmental expression of mouse Kruppel-like transcription factor KLF7 suggests a potential role in neurogenesis. *Dev Biol* 233: 305-318.
116. Groschel, M. I., F. Sayes, R. Simeone, L. Majlessi, and R. Brosch. 2016. ESX secretion systems: mycobacterial evolution to counter host immunity. *Nat Rev Microbiol* 14: 677-691.
117. Prosser, G., J. Brandenburg, N. Reiling, C. E. Barry, 3rd, R. J. Wilkinson, and K. A. Wilkinson. 2017. The bacillary and macrophage response to hypoxia in tuberculosis and the consequences for T cell antigen recognition. *Microbes Infect* 19: 177-192.
118. Cramer, T., Y. Yamanishi, B. E. Clausen, I. Forster, R. Pawlinski, N. Mackman, V. H. Haase, R. Jaenisch, M. Corr, V. Nizet, G. S. Firestein, H. P. Gerber, N. Ferrara, and R. S. Johnson. 2003. HIF-1alpha is essential for myeloid cell-mediated inflammation. *Cell* 112: 645-657.
119. Sherman, D. R., M. Voskuil, D. Schnappinger, R. Liao, M. I. Harrell, and G. K. Schoolnik. 2001. Regulation of the Mycobacterium tuberculosis hypoxic response gene encoding alpha -crystallin. *Proc Natl Acad Sci U S A* 98: 7534-7539.
120. Boshoff, H. I., and C. E. Barry, 3rd. 2005. Tuberculosis - metabolism and respiration in the absence of growth. *Nat Rev Microbiol* 3: 70-80.
121. Trunz, B. B., P. Fine, and C. Dye. 2006. Effect of BCG vaccination on childhood tuberculous meningitis and miliary tuberculosis worldwide: a meta-analysis and assessment of cost-effectiveness. *Lancet* 367: 1173-1180.
122. Mollenkopf, H. J., M. Kursar, and S. H. Kaufmann. 2004. Immune response to postprimary tuberculosis in mice: Mycobacterium tuberculosis and Mycobacterium bovis bacille Calmette-Guerin induce equal protection. *J Infect Dis* 190: 588-597.
123. Ronan, E. O., L. N. Lee, P. C. Beverley, and E. Z. Tchilian. 2009. Immunization of mice with a recombinant adenovirus vaccine inhibits the early growth of Mycobacterium tuberculosis after infection. *PLoS One* 4: e8235.
124. Santosuosso, M., S. McCormick, X. Zhang, A. Zganiacz, and Z. Xing. 2006. Intranasal boosting with an adenovirus-vectored vaccine markedly enhances protection by

parenteral Mycobacterium bovis BCG immunization against pulmonary tuberculosis. *Infect Immun* 74: 4634-4643.
125. Turner, D. L., M. Goldklang, F. Cvetkovski, D. Paik, J. Trischler, J. Barahona, M. Cao, R. Dave, N. Tanna, J. M. D'Armiento, and D. L. Farber. 2018. Biased Generation and In Situ Activation of Lung Tissue-Resident Memory CD4 T Cells in the Pathogenesis of Allergic Asthma. *J Immunol* 200: 1561-1569.
126. Murray, H. W., A. D. Luster, H. Zheng, and X. Ma. 2017. Gamma Interferon-Regulated Chemokines in Leishmania donovani Infection in the Liver. *Infect Immun* 85.
127. Sauer, S., L. Bruno, A. Hertweck, D. Finlay, M. Leleu, M. Spivakov, Z. A. Knight, B. S. Cobb, D. Cantrell, E. O'Connor, K. M. Shokat, A. G. Fisher, and M. Merkenschlager. 2008. T cell receptor signaling controls Foxp3 expression via PI3K, Akt, and mTOR. *Proc Natl Acad Sci U S A* 105: 7797-7802.
128. Muller, A. J., O. Filipe-Santos, G. Eberl, T. Aebischer, G. F. Spath, and P. Bousso. 2012. CD4+ T cells rely on a cytokine gradient to control intracellular pathogens beyond sites of antigen presentation. *Immunity* 37: 147-157.
129. Srivastava, S., P. S. Grace, and J. D. Ernst. 2016. Antigen Export Reduces Antigen Presentation and Limits T Cell Control of M. tuberculosis. *Cell Host Microbe* 19: 44-54.